Article

The (*E*, *Z*) Isomerization of *C*-methoxycarbonyl-*N*-aryl Chlorohydrazones

Giorgio Molteni [1] , **Fausto Cargnoni** [2], **Raffaella Soave** [2] **and Alessandro Ponti** [2,*]

[1] Dipartimento di Chimica, Università degli Studi di Milano, Via C. Golgi 19, 20133 Milano, Italy
[2] Istituto di Scienze e Tecnologie Chimiche "Giulio Natta", Consiglio Nazionale delle Ricerche, Via C. Golgi 19, 20133 Milano, Italy
* Correspondence: alessandro.ponti@scitec.cnr.it

Abstract: Since chlorohydrazones are planar molecules, it is in principle possible to distinguish between their *E* and *Z* stereoisomers. Chlorohydrazones are known to preferentially assume the *Z* configuration around the C=N double bond, and their (*E*, *Z*) isomerization is almost suppressed at room temperature. The lack, or rather the difficulty, of such an isomerization has been conveniently addressed by the in-depth theoretical study of seven *C*-methoxycarbonyl-*N*-aryl chlorohydrazones (aryl = phenyl, 4-chlorophenyl, 4-bromophenyl, 4-iodophenyl, 2-chlorophenyl, 2-bromophenyl, and 2-iodophenyl). DFT ωB97M-D4/cc-pVTZ calculations of these *C*-methoxycarbonyl-*N*-aryl chlorohydrazones, supported by the XRD determination of the molecular structure, provided a complete picture of the isomerization processes in the studied compounds. The analysis of the energetics, molecular geometry, and electronic structure (the latter in the framework of the Quantum Theory of Atoms In Molecules) showed that the *Z* isomers are thermodynamically favored because, within the low-energy planar isomers with extensive π conjugation, the electrostatic interactions between the dipoles of the C–O, C–Cl, and N–H bonds overcome the stabilization induced by the N–H $\cdots$ O bond present in the *E* isomers. We confirmed that the (*E*, *Z*) isomerization occurs by the *umklapp* mechanism, in which the –NHAr moiety rotates in the molecular plane towards a linear C=N–N configuration and then proceeds to the other isomer. The (*E*, *Z*) isomerization is very slow at room temperature because the *umklapp* interconversion has high barriers ($\approx$110 kJ/mol) despite the extended π electron delocalization present in the transition state.

Keywords: chlorohydrazones; (*E*, *Z*) isomerization; DFT calculation; ωB97M; QTAIM; X-ray diffraction

1. Introduction

Hydrazonoyl halides or halohydrazones were first prepared by Fisher in 1882 [1]. They are characterized by the presence of a –C(X)=N–NH– moiety [2–7], where X is usually a chlorine or bromine atom. Iodohydrazones are very rare, the first example was published in 2008 [8], and no fluorohydrazones are known.

In support of their multiple uses, hydrazonoyl halides have recently been defined as a "bubbling fountain of biologically active compounds" [9]. The main uses of chlorohydrazones are related to their activity as phytotoxic agents, particularly herbicides [10] and insecticides, since they act as plant growth regulators in rather small amounts, typically between 0.01 and 10^{-5} wt% relative to the green part of the plant [11]. Those chlorohydrazones also have proven to be very useful insecticides due to their activity in inhibiting the metamorphosis of insects, particularly the cabbage mite, which belongs to the lepidopteran family [12]. Further examples of hydrazonoyl halides bioactivity are concerned with their anthelmintic activity in the veterinary field [13], as well as fungistatic and bactericidal activity [14]. More recently, the cytotoxic activity of some chlorohydrazones against colon cancer cell lines has emerged. IC50 values showed significant cell apoptosis, with values less than 20 μM for all human cancer cell lines considered [15]. As an adverse effect, cases of severe dermatitis caused by chlorohydrazone PhC(Cl)=N-NHPh have been reported [16].

As a result of the exchangeability of the N–H proton with D_2O, it is possible to obtain deuterated halohydrazones useful in mechanistic studies. This mobile proton gives the chlorohydrazones an acidity comparable to those of the corresponding phenols [17]. In accordance with their acidic properties, the main feature of the chemistry of hydrazonoyl halides is configured in their dehydrohalogenation, which occurs readily in the presence of a base [18]. The result of dehydrohalogenation involves the generation of the corresponding nitrilimine –C≡N⁺–N⁻– as an unstable and generally non-isolable 1,3-dipole [19]. From the synthetic point of view, nitrilimines constitute the key intermediate in the construction of the pyrazole ring [2–7,18,19].

Analytically pure chloro- and bromo-hydrazones usually occur as amorphous solids with a sharp melting point, are stable in air and storable at room temperature, and have poor solubility in hydrocarbon solvents and good solubility in chlorinated solvents, with the exception of carbon tetrachloride [2–7]. In rather rare cases, it has been possible to obtain crystalline-state samples from which the corresponding detailed structures could be obtained through X-ray diffraction experiments [20]. The molecules of halohydrazones are generally planar but it is in principle possible to distinguish between the *E* and *Z* stereoisomers due to the presence of the C=N double bond. Hydrazonoyl halides preferentially assume the *Z* form, as suggested by spectroscopic studies [21] and X-ray diffractometric (XRD) analyses [20]. *Z* isomers are thermodynamically more stable than the corresponding *E* isomers, and interconversion between the two forms occurs very slowly compared to the similar equilibrium involving simple imine derivatives [22,23]. Nonetheless, it is possible to imagine that with appropriate substituents on the iminic carbon it would be possible to extend the properties of chemically controlled configurational rotary switches to chlorohydrazones, as known in the case of *C,N*-diarylhydrazones [24].

In the case of *C*-methoxycarbonyl-*N*-aryl chlorohydrazones **1–7** that are considered in the present paper (Figure 1), the absence of the *E* isomer has been explained by admitting that the intramolecular N–H ⋯ O hydrogen bond, seemingly effective in *E* isomers (Figure 1), does not intervene. This statement is consistent with XRD and infrared (IR) data for the N–H bond stretching vibration of oxanilo-*N*-arylhydrazonoyl chlorides [20], but is in contrast with data for phenylhydrazone derivatives of alloxan [25].
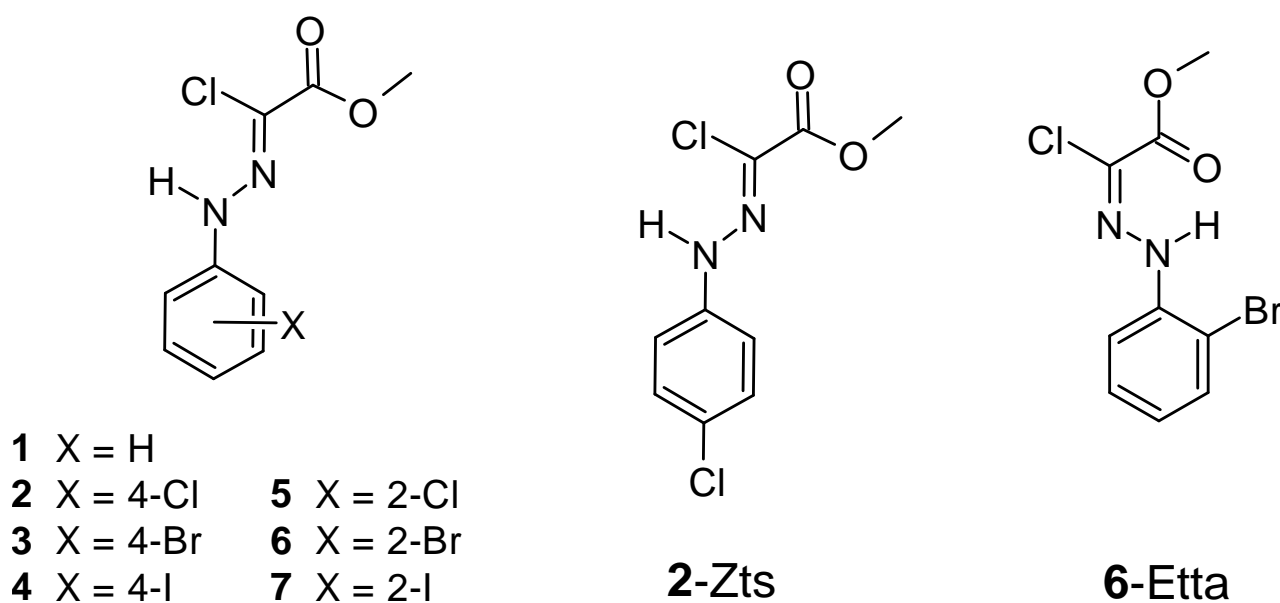

1 X = H
2 X = 4-Cl   **5** X = 2-Cl
3 X = 4-Br   **6** X = 2-Br
4 X = 4-I   **7** X = 2-I

2-Zts   **6**-Etta

Figure 1. The seven investigated chlorohydrazones and two particular isomers of **2** and **6**.

Surprisingly, besides the mentioned experimental data that provide insights into the structure of hydrazonic halides, the theoretical aspect of their (*E*, *Z*) isomerization has not yet been conveniently addressed. The purpose of the present article is therefore the in-depth

theoretical study of this isomerization referring to chlorohydrazones **1–7**, duly supported by diffractometric experimental data. In particular, we will focus on the following issues: (i) why is the *Z* isomer thermodynamically favored? (ii) Is the intramolecular N–H ⋯ O hydrogen bond effective? (iii) Why is the (*E*, *Z*) isomerization so slow (Figure 2) to escape detection?
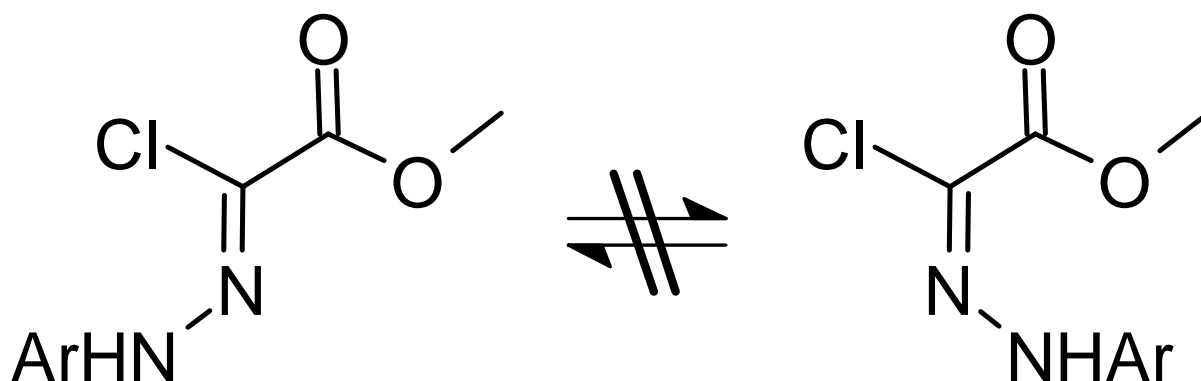

Figure 2. Lack of *E-Z* isomerization for *C*-methoxycarbonyl-*N*-aryl chlorohydrazones.

2. Methods

2.1. X-ray Diffraction

Single-crystal X-ray diffraction data were collected for compounds **1** and **3** at room temperature (293(2) K) on a three-circle Bruker SMART APEX II diffractometer equipped with a CCD area detector. Diffraction data were recorded using ω-scans (0.5 deg/frame) with graphite monochromated Mo Kα radiation (λ = 0.71073).

Compound **1**: Plate-shaped light orange single crystals were grown by slow evaporation of a mixture (1:1) of CH_2Cl_2/hexane at 25 °C. A total of 18008 X-ray diffraction data were collected up to a 2θ Bragg angle of 61.0°. Crystal structure data have been deposited at the Cambridge Crystallographic Data Centre and allocated the deposition number CCDC 2212526. The deposited CIF is included in the Supplementary Materials.

Compound **3**: Prism-shaped pale yellow single crystals were grown by slow evaporation of a mixture (1:1) of CH_2Cl_2/hexane at 25 °C. A total of 103976 X-ray diffraction data were collected up to a 2θ Bragg angle of 90.6°. Crystal structure data have been deposited at the Cambridge Crystallographic Data Centre and allocated the deposition number CCDC 2212525. The deposited CIF is included in the Supplementary Materials.

2.2. Computational Methods

DFT calculations using the M08-HX functional [26] and the cc-pVDZ and cc-pVTZ basis sets [27,28] were carried out using Gaussian16 A.03 (Gaussian: Gaussian Inc., Wallingford, CT, USA) [29], calculations using the ωB97M-D4 functional [30,31] and the cc-pVTZ basis set were carried out using ORCA 5.0.3 (Max-Planck-Institut fuer Kohlenforschung, Muelheim a. d. Ruhr, Germany) [32]. Calculations of molecules containing Br or I atoms were carried out using SK MCDHF RSC pseudo-potentials [33] and the cc-pVDZ-PP and cc-pVTZ-PP basis sets [34,35] for Br and I. Isomer minimum energy and TS structures were fully optimized with tight thresholds for both SCF and geometry optimization. Harmonic analysis in the RRHO approximation confirmed the minimum of TS nature of all structures. IRC analysis was used to ascertain which isomers correspond to selected TSs.

The QTAIM analysis of the electron density of selected minimum energy isomers and TSs was carried out adopting the Multiwfn computational code [36]. Bond critical points of the electron density have been located using the midpoint of atom pairs as starting guesses. The search for secondary interactions has been refined using selected points in space as a guess for the location of bond critical points. We are therefore confident that the presence or the absence of secondary interactions has been recovered correctly. As for atomic properties,

we located attractors and defined atomic basins surfaces using a high-quality grid. The overall charge of the molecule, estimated as the sum of atomic charges, deviates from neutrality by a few hundredths of electron, which is an indicator of the accuracy of the data presented here. As an additional tool to provide an interpretation of the energy ordering among isomers, we computed the Delocalization Index (DI) between selected couples of atomic basins. The DI provides a rigorous measure of the interaction between atoms in terms of electron pairing [37,38] and proved useful also in studies of secondary interactions such as hydrogen bonds [39,40].

The Kinetic Monte Carlo (KMC) simulations were carried out by an in-house Matlab® implementation of the Gillespie algorithm [41]. The rate constants were calculated using the Eyring formula $k = \kappa\,(k_B T/h)\,\exp(-\Delta G^{\ddagger}/RT)$ with $\kappa = 1$ and $T = 298$ K and the $\Delta G^{\ddagger}$ activation barriers calculated at the ωB97M-D4/cc-pVTZ level of theory. Simulations were carried out with initial conditions consisting of pure **1**-Eta or **1**-Zts isomers. Due to the huge differences among the isomerization rate constants, we were forced to assume fast thermal equilibration within the **1**-Et(a,s) or **1**-Zt(a,s) pairs, respectively, in order to observe the isomerization of interest within a reasonable computation time (1–2 weeks).

3. Results and Discussion

3.1. Structure and Energetics of the Isomers of Chlorohydrazones **1**–**7**

3.1.1. Generalities

The investigated chlorohydrazones (Figure 1) feature (*E*, *Z*) geometric isomers because of the presence of the C=N double bond. Furthermore, rotation about the formally single Ar–N, N–N, C–COOMe, and C–OMe is restricted, as we will shortly show. Thus, the chlorohydrazones have well-defined pairs of energy minima for rotation about these bonds, corresponding to pairs of isomeric structures. Of course, the rotation of the methyl group can be considered free at RT.

The isomers arising from the two possible orientations of the Me group (rotation about C-OMe) will not be considered further because of the limited chemical significance of this isomerism. Suffice to say that the isomer with the Me group close to the carbonyl group is always the more stable. The free energy difference ΔG is $\approx$40 kJ/mol. Therefore, only the more stable isomer is appreciably populated. The present consideration allows us to somewhat reduce the complexity of the isomerization landscape.

Taking into account the (*E*, *Z*) isomerism and the restricted rotations about the Ar–N, N–N, and C–COOMe bonds, chlorohydrazones **1**–**7** give rise to 16 possible isomers that we denote as **n**-Φθψγ, where **n** = **1** to **7** denotes the chlorohydrazone and the symbols Φ, θ, ψ, and γ denote the isomers, where Φ = E or Z, the geometric isomers; θ = c(isoid) or t(ransoid), the conformers about the N-N bond; ψ = c or t, the conformers about the Ar-N bond; and γ = a(nti) or s(yn), the conformers about the C-COOMe bond, as explained in Table 1. Precedence is determined following the Cahn–Ingold–Prelog rules. We use the old-fashioned cisoid/transoid terms to make the notation perspicuous. The different nomenclature for the C-COOMe isomerism is due in part to the smaller free energy difference and activation barrier for these isomers, and in part to make notation clearer. The ψ isomerism is not present in **1**–**4** and they are therefore denoted as **n**-Φθγ. As examples, the **2**-Zts and **6**-Etta isomers are depicted in Figure 1. The planar or dihedral angles related to the isomeric pairs will also be denoted as Φ, θ, ψ, and γ. We wondered why chlorohydrazones **3** and **6** occur in solution as the Z isomer despite the facts that (i) a hydrogen bond between the N–H hydrogen atom and either of the O atoms in the ester group can likely form in the E isomers and (ii) there is no obvious reason why the Z isomers should be preferred.

Table 1. Definition of the nomenclature for the chlorohydrazone isomers.

	Definition	Typical Values	
Φ	C=N–N	≈120°, *Z*	≈240°, *E*
θ	C–N–N–Ar	≈0°, *c(isoid)*	≈180°, *t(ransoid)*
ψ	N–N–C_{ipso}–C_{ortho}	≈0°, *c(isoid)*	≈180°, *t(ransoid)*
γ	Cl–C–C=O	≈0°, *s(yn)*	≈180°, *a(nti)*

3.1.2. Crystal Structure of Chlorohydrazones **1** and **3**

The molecular structure in the solid state of compounds **1** and **3** has been investigated through single-crystal X-ray diffraction experiments. Both compounds crystallize in the orthorhombic crystal system with space groups P_{212121} and Pbca, respectively. Figure 3 shows the molecular conformations of the two compounds in the solid state. In both cases the Zts isomer is observed with Φ = 121.65(16) and 120.02(18) deg, for **1** and **3**, respectively. The θ torsion angles about the N–N bond (see previous section for definition) amount to 178.04(18) and 173.19(19), respectively, indicating that in the solid state the θ = *t(ransoid)* conformers are present, with a small distortion in the case of **3**, which is likely due to the accommodation of the large Br atom in the crystal lattice. In both crystals, the molecules are almost completely planar. The full list of torsion angles can be found in the Supplementary Materials and the deposited CIF (CCDC 2212526 and CCDC 2212525). Intermolecular N–H ··· O=C hydrogen bonds are present in both crystal structures and closely resemble the packing patterns reported by Frohberg et al. [20]. No intramolecular H-bond is present, as expected for the Zts isomer.
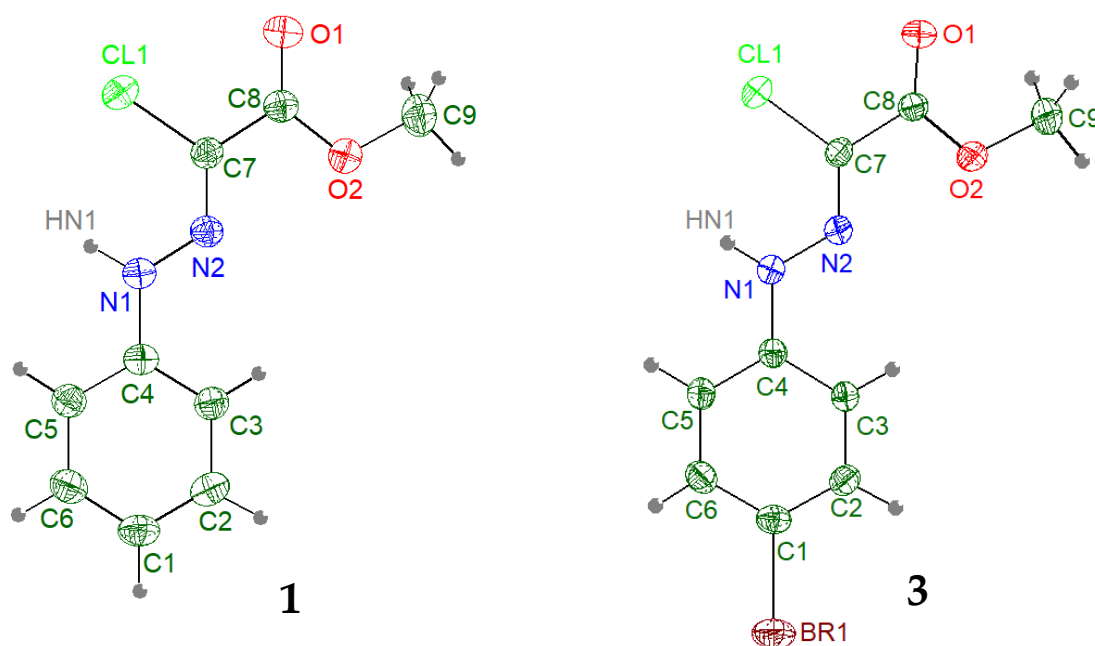
Figure 3. ORTEP plot of **1** and **3**. Anisotropic displacement parameters are at the 50% probability level.

Crystal packing of compound **1** down *c* and *a* axes together with relevant intermolecular interactions are reported in Figure 4. The overall motif is that of zigzag ribbons extended along the *b* axis. Geometrical parameters for the N–H ··· O=C intermolecular hydrogen bond which packs together molecules in the crystallographic *bc* plane are as follows: d [HN1···O1(−x, y + $\frac{1}{2}$, −z + 3/2)] = 2.210(2) Å; N1-HN1···O1(−x, y + $\frac{1}{2}$, −z + 3/2) = 159.64(10) deg.
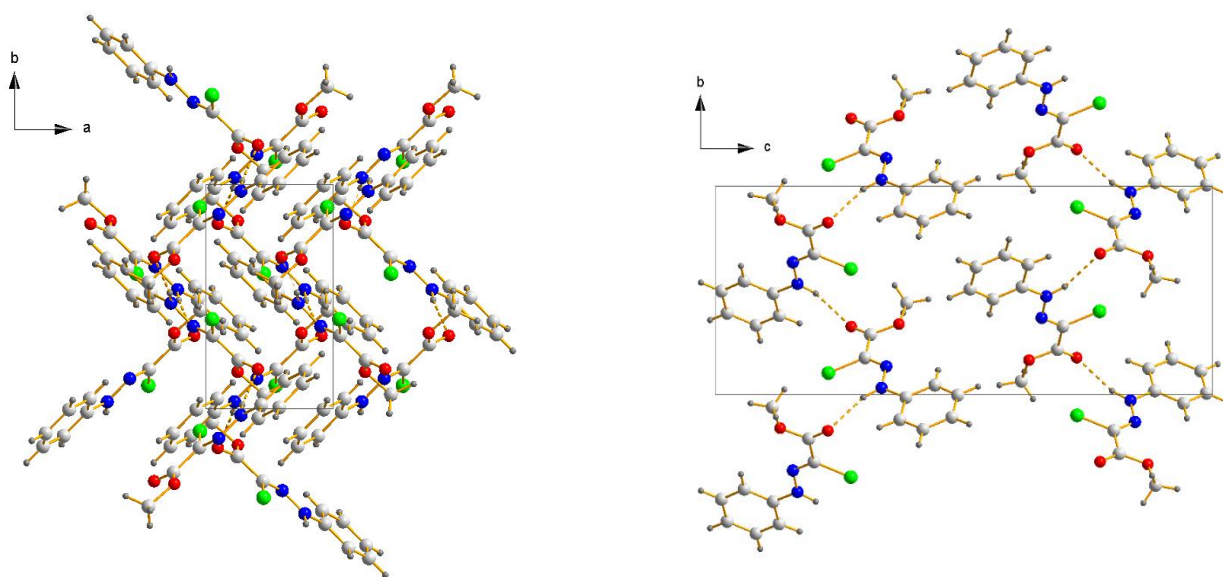
Figure 4. Crystal packing views down the *c* (**left**) and *a* (**right**) axis for compound **1**.

In Figure 5 (left), the crystal packing of compound **3** viewed down the *a* axis is shown. Again, a zig-zag pattern is observed extending along the *c* direction and with the molecular plane forming an angle of about 90 deg with the crystallographic *bc* plane. Figure 5 (right) shows the dimer, which forms because of the N1-HN1···O1 intermolecular hydrogen bond. The oxygen acceptor atom belongs to the equivalent molecule in $(-x + 1, y + \frac{1}{2}, -z - \frac{1}{2})$. The zig-zag motif is quite common in molecular crystals of small organic molecules, such as hydrazones or naphtoquinone [42,43].
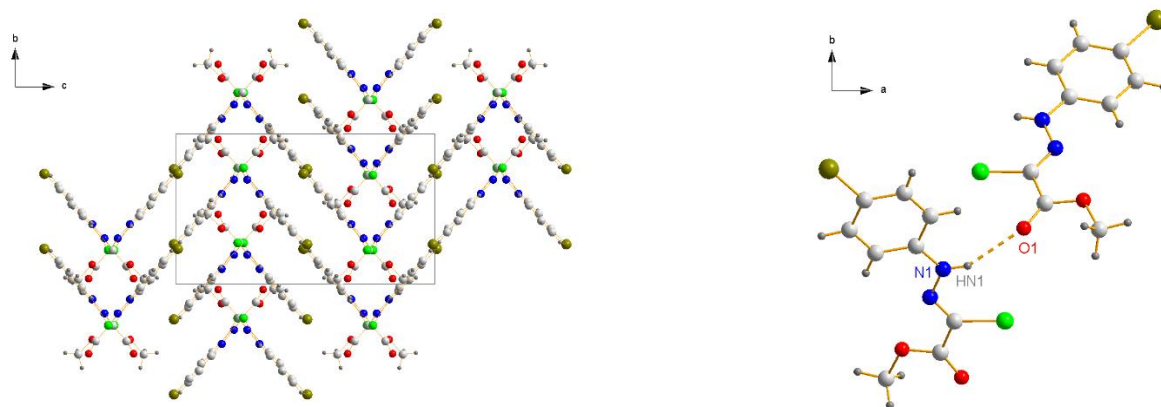

Figure 5. Partial crystal packing views down the *a* (**left**) and *c* (**right**) axis for compound **3**.

3.1.3. DFT Structure and Energetics of the Isomers of Chlorohydrazone **1**

Species **1**–**4** can have 8 minimum energy structures, whereas species **5**–**7** can have 16 minimum energy structures, totaling 80 minimum energy structures. We first made a thorough DFT investigation of the isomers of **1**–**7** at the M08HX/cc-pVDZ, M08HX/cc-pVTZ, and ωB97M-D4/cc-pVTZ level of theory. The energetic and structural comparison in the Supplementary Materials (Tables S4–S21 and Figures S1–S12) shows that the computational results are robust, i.e., that the qualitative picture of the chlorohydrazone isomerism is not different for different levels of theory and that the quantitative differences in isomer structure, energetics, population, and interconversion rate are reasonably small.

The minimum energy structures of **1**, calculated at the ωB97M-D4/cc-pVTZ level, are depicted in Figure 6, and their relative free energies and populations can be found in Table 2 and Figure 7.
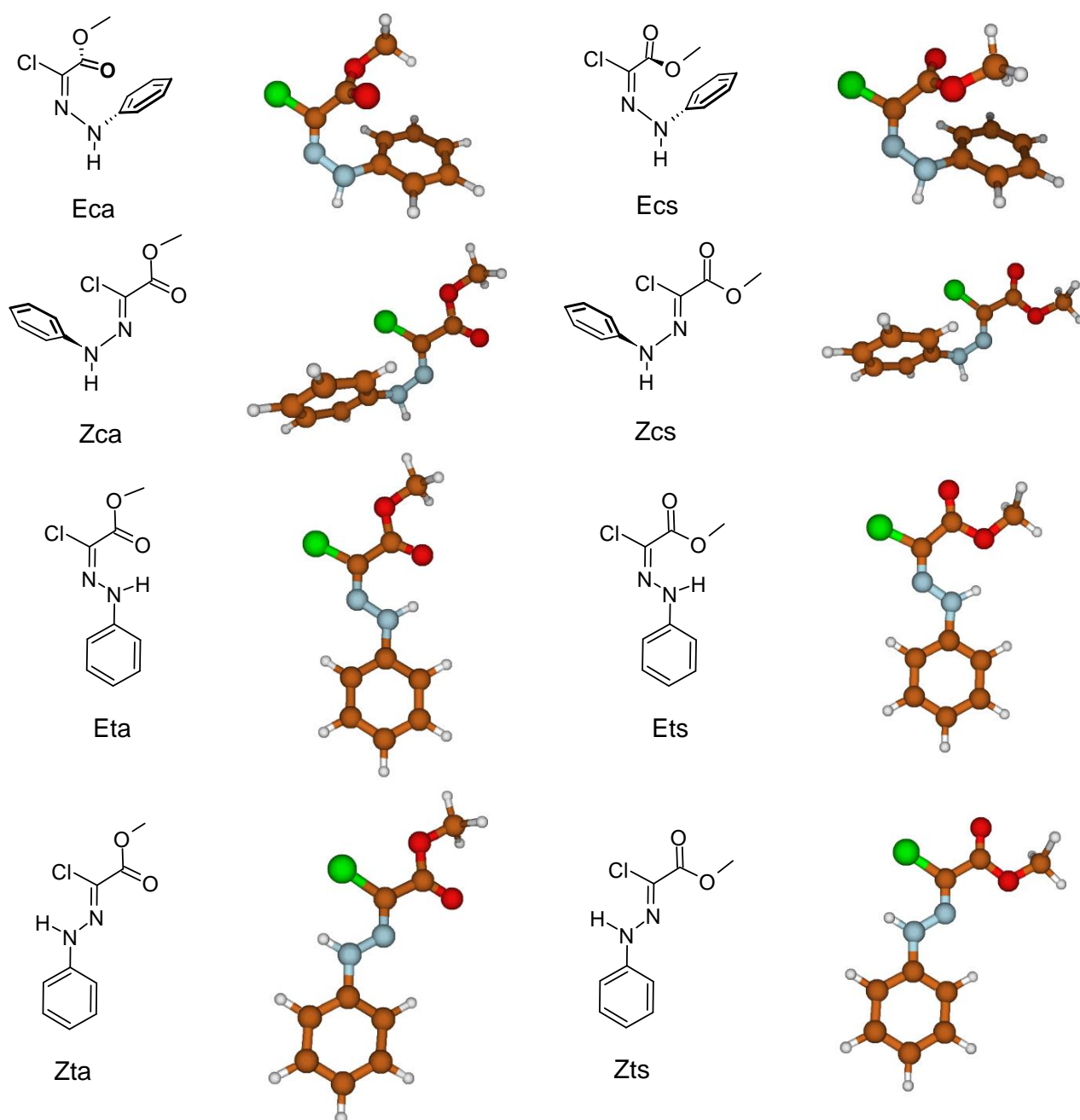
Figure 6. Minimum energy structures of **1** calculated at the ωB97M-D4/cc-pVTZ level.

Table 2. Energetics of the minimum energy structures of **1** calculated at the ωB97M-D4/cc-pVTZ level. The reaction free energy Δ*G* (kJ/mol) is listed along with the relative population at 298 K.

	Δ*G* (kJ/mol)	Rel. Pop.
Eca	54.9	$1.7 \cdot 10^{-10}$
Ecs	54.3	$2.2 \cdot 10^{-10}$
Eta	6.4	0.06
Ets	22.4	$8.6 \cdot 10^{-5}$
Zca	45.9	$6.7 \cdot 10^{-9}$
Zcs	42.8	$2.3 \cdot 10^{-8}$
Zta	3.0	0.22
Zts	0.0	0.73

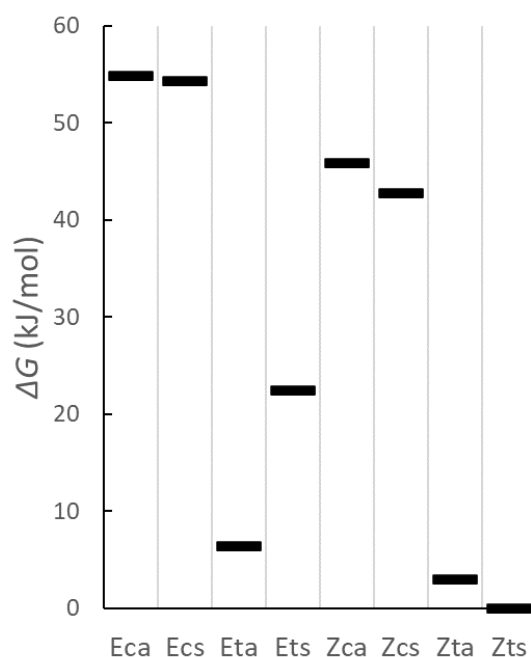**Figure 7.** Relative free energy at 298 K of the minimum energy structures of **1** calculated at the ωB97M-D4/cc-pVTZ level. The vertical lines are just a guide for the eye.

The most stable isomer at 298 K is Zts, which is the isomer observed by XRD in the crystal of **1**. The calculated structure of **1**-Zts is very close to the experimental one, as can be appreciated from Table 3. The isomers with appreciable population at 298 K are Zts, Zta, and Eta. The other isomers have a population from 4 to 9 orders of magnitude smaller. The *Z* isomers account for 95% of the **1** molecules, in agreement with previous findings [20,21]. Unexpectedly, Table 2 and Figure 7 show that the main energetic difference is between θ isomers, with **1**-Φtγ favored by ≈50 kJ/mol with respect to the corresponding **1**-Φcγ. These peculiar energetics are closely related to the isomer molecular geometry (Figure 6). All **1**-Φtγ isomers are planar, while in the **1**-Φcγ isomers the phenyl ring is tilted by |θ| = 40–50° with respect to the hydrazone moiety (Table 3) due to steric interaction between the phenyl ring and either the Cl atom or the COOMe group. **1**-Z isomers are more stable that the corresponding *E* isomers by ≈20 kJ/mol with the exception of the **1**-(E,Z)ta pair. This exception is caused by the substantial stabilization of **1**-Eta with respect to **1**-Ets (16 kJ/mol), much larger than the difference between other *syn* (favored) and *anti* conformers that amount to a few kJ/mol. We now analyze in more detail the energetics of each isomerism and try to answer questions (i) and (ii) that were posed in the Introduction.

Table 3. Selected molecular geometric parameters of the minimum energy structures of **1** calculated at the ωB97M-D4/cc-pVTZ level compared with those determined by XRD. Bond lengths are in angstroms, planar and dihedral angles are in degrees.

	C=N	N-N	N-C$_{ipso}$	Φ	θ	ψ	δΣ
Eca	1.259	1.362	1.433	238.2	−38.9	−33.7	15.3
Ecs	1.260	1.362	1.431	237.3	−40.1	−29.0	14.8
Eta	1.277	1.314	1.402	237.4	178.9	0.9	0.0
Ets	1.271	1.317	1.401	235.1	178.8	1.3	0.0
Zca	1.262	1.351	1.433	123.7	−49.7	−23.8	16.1
Zcs	1.263	1.356	1.434	123.0	−51.0	−23.8	17.0
Zta	1.268	1.314	1.402	121.4	181.2	0.0	0.0
Zts	1.268	1.317	1.401	121.1	180.6	1.3	0.0
XRD (Zts)	1.270(2)	1.321(2)	1.402(2)	121.65(16)	178.04(18)	−0.3(3)	0.2

δΣ is the the difference δΣ = 360° − Σ, where Σ is the sum of the planar angles about the –NH–atom.

Energetics of the θ (c, t) Isomerism

It is natural to think that the importance of θ isomerism about the N-N bond is related to the conjugation (π electron delocalization) between the π electron systems of the phenyl ring and N=C–C=O hydrazonic skeleton. However, the conjugation seems to occur through the formally sp^3 –NH– nitrogen atom. We now support the conjugation hypothesis with reference to structural data, and in the following we will give more stringent proof based on the QTAIM analysis of the electronic structure. As can be seen in Table 3, the length of the C=N bond is almost constant across the isomers of **1**. It is slightly longer in the **1-Φtγ** than in the **1-Φcγ** isomers, hinting at a slightly higher C=N bond order in the latter. The length of the N–N bond is significantly different between the planar **1-Φtγ** (≈1.31 Å) and non-planar **1-Φcγ** (≈1.36 Å) isomers. We can compare those with the length of the N–N bond in dinitrogen compounds (Table 4). The N–N length of **1** is between those of phenyl hydrazine and (phenyl)diazene indicating a partial double bond character. The latter is much larger for the **1-Φtγ** isomers, in which the N-N bond length is closer to that of (phenyl)diazenes than that of phenyl hydrazine. The length of the N–C_{ipso} bond of **1-Φtγ** isomers is ≈0.3 Å shorter than that of **1-Φcγ** isomers, again hinting at a higher bond order in θ = t isomers. In summary, structural data suggests that the N–N and N–C_{ipso} bonds have partial double bond character in **1-Φtγ** isomers, relating to a larger sp^2 character of the aminic N atom and improved conjugation. The C=N bond is longer in **1-Φtγ** hinting at a lower bond order, in agreement with extended π conjugation to the whole molecule.

Table 4. Length of the N-N bond (Å) in selected small molecules, calculated at the ωB97M-D4/cc-pVTZ level.

	N-N
$H_2N–NH_2$	1.476
$H_2N–NHPh$	1.407
HN=NH (*Z*)	1.233
HN=NH (*E*)	1.235
HN=NPh (*Z*) [a]	1.236
HN=NPh (*E*) [b]	1.232
N≡N	1.091

[a] Planar structure. [b] Non-planar structure.

To clarify the picture, we calculated the sum, Σ, of the planar angles about the –NH– atom and the difference, $δΣ = 360° − Σ$, the latter being 0° for a planar coordinated sp^2 atom and ≈29° for the pyramidal sp^3 N atom of $NHMe_2$. δΣ is 0.0° for the **1-Φtγ** isomers and is in the 10–20° range for the **1-Φcγ** isomers. Therefore, δΣ indicates that the –NH– nitrogen atom is sp^2 in **1-Φtγ** whereas it has mixed sp^3/sp^2 character in **1-Φcγ**, in agreement with the conjugation hypothesis. In conclusion, structural data provide significant (though not conclusive) proof that the stabilization of the **1-Φtγ** isomers is due to π conjugation between the phenyl ring and the rest of the chlorohydrazone. The **1-Φcγ** isomers seem to retain some molecule-wide conjugation despite their non-planar structure.

Energetics of the γ (a, s) Isomerism

The next point worth discussing is why **1-Etα** is more stable by 16.0 kJ/mol than **1-Ets**. By inspecting Figure 6, it is clear that only in the **1-Etγ** isomers a N–H ⋯ O interaction can be established. The H ⋯ O distance (1.904 and 1.951 Å in **1-Eta** and **1-Ets**, respectively) is well below the sum of the H and O van der Waals radii (1.10 + 1.52 = 2.62 Å) [44], so this satisfies the distance requirement for a real hydrogen bond.

The H-bond in **1-Eta** is stronger, as supported by the larger N–H distance (**1-Eta**: 1.012 Å, **1-Ets**: 1.008 Å) and lower calculated N–H stretching frequency (**1-Eta**: 3518.9 cm^{-1}, **1-Ets**: 3591.3 cm^{-1}). The H-bond in **1-Eta** involves the sp^2 carbonyl oxygen and is therefore expected to be stronger [45]. In the present case, both **1-Et(a,s)** are planar and the N–H hydrogen points towards the maximum of the oxygen lone-pair sp^2 orbital in **1-Eta**, but it

points just between the two oxygen lone-pair sp^3 orbitals in **1**-Ets. We will shortly present further evidence supporting the existence of a real H-bond in **1**-Etγ.

Energetics of the Φ (E, Z) Isomerism

The chemically most interesting point is why **1**-Z$\theta\gamma$ isomers are more stable than the corresponding **1**-E$\theta\gamma$ isomers. For the θ = c isomers, not populated at 298 K, it is sufficient to note that destabilizing steric effects are more important in the crowded **1**-Ecγ isomers. It is more interesting to wonder why **1**-Ztγ have lower free energy than **1**-Etγ despite the presence of the hydrogen bond in the latter.

To clarify this point, we calculated the energetics of the systems depicted in Figure 8, where the Cl atom of **1** was replaced with a H atom, or the COOMe group was replaced with a Me group, or both. These systems are denoted as pro-(E, Z) meaning that the systems derived from, e.g., **1**-Ztγ by replacement of R^1 or R^2, are denoted pro-Z irrespective of the priority of R^1 and R^2. The ωB97M-D4/cc-pVTZ energetics of the four R^1 = (H, Cl) and R^2 = (Me, COOMe) cases are collected in Table 5. With reference to the $\Delta G(Z–E)$ difference for the (R^1 = H, R^2 = Me) case, one can see that introducing the R^2 = COOMe group favors the *E* isomer by 24.2 kJ/mol. Indeed, 2-bromo-1-phenylglyoxal 2-phenylhydrazones, which have an α carbonyl but no α halogen, prevailingly exist in the *E* configuration [46]. Introducing the R^1 = Cl atom favors the *Z* isomer by 23.2 kJ/mol. When both Cl and COOMe are present (i.e., in **1**-(E,Z)ta), *Z* is favored by 0.3 kJ/mol, which is not far from the algebraic sum of the two effects (+1.0 kJ/mol). Then, the two effects are approximately independent. Stabilization of the *E* isomer by R^2 = COOMe is easily explained by the formation of a N–H $\cdots$ O H-bond between the COOMe and the –NH– hydrogen atom. Conversely, why R^1 = Cl strongly favors the *Z* isomer is far less clear.
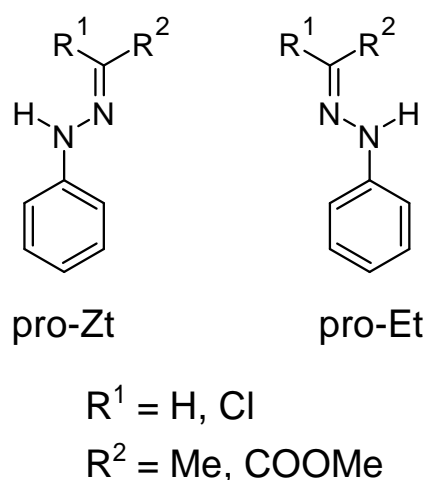

R^1 = H, Cl
R^2 = Me, COOMe

Figure 8. Model systems used to investigate the (*E*, *Z*) isomerism of **1**.

Table 5. Free energy difference between *Z* and *E* isomers of the pro-systems, calculated at the ωB97M-D4/cc-pVTZ level.

R^1	R^2	$\Delta G(Z–E)$ (kJ/mol)	Z Fraction [a]
H	Me	1.7	67%
H	COOMe [b]	–22.5	0%
Cl	Me	24.9	100%
Cl	COOMe [b,c]	2.0	69%

[a] Fraction of the Z isomer at 298 K, referred to the (E, Z)t pair only. [b] γ = anti. [c] This is the **1**-(E, Z)ta pair.

In conclusion, the presence of the Cl atom induces a stabilization of the populated *Z* isomers. The physical basis for this will be unveiled by the QTAIM analysis below. This stabilization is almost counterbalanced by the stabilization induced by the H-bond present

in **1**-Eta, which is 6.4 kJ/mol higher than **1**-Zts and thus is appreciably populated (5%) at 298 K.

3.1.4. Electronic Structure and π Delocalization of the Isomers of Chlorohydrazone **1**

The envisaged conjugation (π electron delocalization) between the aryl and hydrazonic moieties through the planar aminic N atom is not alien to a naive Lewis structure picture where it forms four bonds and assumes a formal positive charge balanced by a negative one residing on the aryl ring or carbonyl group (Figure 9).
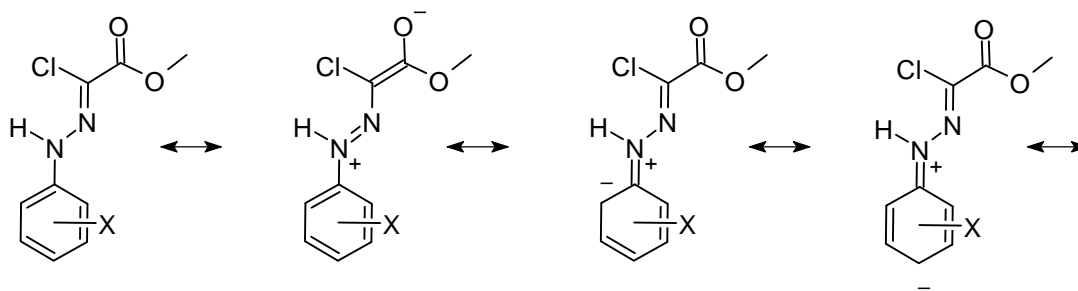

Figure 9. Lewis structures of chlorohydrazones **1**–**7**, including zwitterionic structures consistent with electron conjugation between the aryl and hydrazonic moieties.

The presence of π occupied orbitals extending over the N–N and N–C_{ipso} bonds (Figures 10 and S3) is consistent with the extended delocalization picture and partial double bond character of the N–N bond.
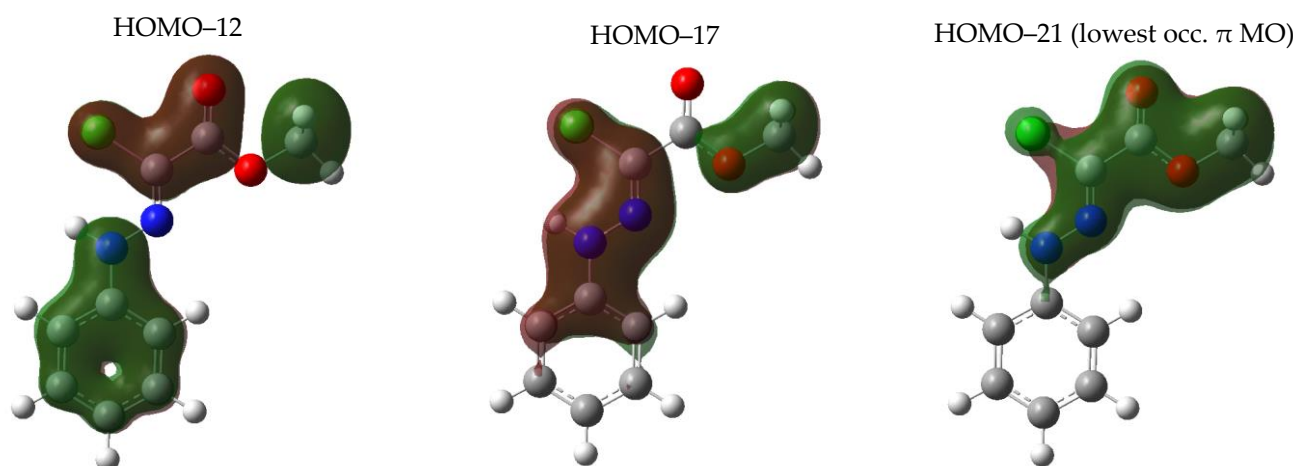
HOMO–12　　　　　　　　HOMO–17　　　　　　HOMO–21 (lowest occ. π MO)

Figure 10. ωB97M-D4/cc-pVTZ MOs showing molecule-wide π delocalization in **1**-Zts.

In this section, we analyze in more detail how the molecular electronic structure determines the energy order of the isomers, adopting the approach of the Quantum Theory of Atoms in Molecules (QTAIM) [47]. We considered the eight isomers of **1**, and conducted the topological analysis of the ωB97M-D4/cc-pVTZ electron density ρ. We characterized the bonding structure in terms of properties of the electron density ρ at the bond critical points (bcp). We also determined the atomic properties by integrating the electron density and its multipolar terms over atomic basins. In the following, we report on the main results in a descriptive fashion, referring the interested reader to the complete set of data collected in the Supplementary Materials; the atomic charges and dipoles are in Table S1 and the properties of bonds relevant for the discussion are in Table S2 (bond length, electron density, Laplacian of the electron density, and bond ellipticity, the latter three calculated at the bond critical point). The delocalization indices (DIs) of selected atoms pairs of the Etγ and Ztγ isomers, which provided a key element to rationalize their energy ordering, are

collected in Table 5, while the complete set of considered DIs is collected in Table S3 of the Supplementary Materials.

The bonding structure of the lowest energy isomer, **1**-Zts, agrees with the one derived from chemical intuition. The π electrons are mostly localized onto the C=N bond, which has the features of a pure double bond, with a large and negative Laplacian of the electron density, $\nabla^2(\rho)$, and a marked ellipticity ($\varepsilon = 0.51$) at the bond critical point due to a preferential distribution of bonding electrons normal to the plane of the molecule. A lower π character is present also in neighboring, formally single C–C and N–N bonds ($\varepsilon = 0.17$ and 0.12, respectively), as well as the C=O bond ($\varepsilon = 0.13$). A residual π character has been found also in the N–C_{ipso}, C–O, and C–Cl bonds. Overall, this picture suggests that, in addition to the π electrons of the sp^2 carbon and nitrogen atoms, the lone electron pairs of the halogen, nitrogen, and oxygen atoms are involved in the extended π bonding network. It is therefore confirmed that the π bonding structure is delocalized over the entire molecule, with the exception of bonds involving hydrogens. As for the atomic properties, the *ipso*, iminic, and carbonyl carbon atoms have a significant positive charge (about +0.3, +0.8, and +1.7 e, respectively), while the nitrogen, chlorine, and oxygen atoms have an excess electronic population ($q = -0.7$, -0.2, and -1.2 electrons for N, Cl, and O, respectively). The polarization of electrons within atomic basins of N, Cl, C, and O atoms, quantified through the evaluation of the atomic electric dipole, counterbalance the electron transfer among atomic basins, as typical of polar covalent bonds. This feature is observed also in the hydrogen atom bonded to the aminic nitrogen; H bears a positive charge of about 0.4 e and has a small atomic dipole of 0.2 a.u., aligned along N–H and directed from N to H, such as to oppose to the net charge transfer from H to N.

As for secondary intramolecular bonds, neither O···H and Cl···H bonds are present. However, the analysis of atomic charges indicates that the C–Cl electric dipole, which points towards C, interacts unfavorably with the nearby and almost parallel C=O dipole, and favorably with the N–H dipole. The latter points towards the hydrogen atom, is smaller, and is located at larger distances from C–Cl than C=O (Figure 6). It is worth noting that a small but non-negligible pairing among electrons of chlorine and N–**H** is present in **1**-Zts (Table 6). Indeed, the DI (Cl, N–**H**) measures 0.051, a value typical of secondary interactions such as hydrogen bonds of medium strength.

Table 6. Delocalization Indices for the non-covalent interactions of the N–**H** hydrogen atom with the chlorine and oxygen atoms of the **1**-Φtγ isomers. One member of the atom pair is always the hydrogen atom bonded to nitrogen, N-**H**, while the other is reported in the first column.

	1-Zts	**1-Zta**	**1-Ets**	**1-Eta**
Cl	0.051	0.051	0.002	0.001
C=**O**	0.001	0.001	0.002	0.075
C–**O**	0.001	0.000	0.062	0.002

The second lowest-lying isomer, **1**-Zta, has the same bonding structure and properties of **1**-Zts. The evaluation of DIs between bonded atom pairs (Table S3) reveals no significant differences with respect to **1**-Zts, with variations of the order of 1% and no evident trend. The higher energy of **1**-Zta can be explained by noting that the strongest dipole–dipole interaction in Ztγ is likely the one involving charge transfers associated to C–Cl and C–O bonds. The increase in energy from **1**-Zts to **1**-Zta is thus explained considering that the net charge separation between carbon and oxygen in C–O is almost equal to C=O (Table S1), but the internuclear distance is about 10% larger in C–O than in C=O (Table S2), leading to a larger dipole and repulsive term upon interaction with C–Cl.

1-Eta and **1**-Ets isomers are less stable than **1**-Zts and **1**-Zta. This might appear as a contradiction of common sense, because in both **1**-Eta and **1**-Ets an intramolecular N–H ··· O hydrogen bond is present, as proved by the presence of a bcp between the H and O atoms. The covalent bonding structure, measured by the DIs (Table S3), presents no

significant differences between **1**-Etγ and **1**-Ztγ. Noticeably, in **1**-Eta and **1**-Ets, the N–H ⋯ O atoms are far from being aligned, i.e., they largely deviate from the most favorable conformation for H-bonding. Acceptor⋯hydrogen–donor angles significantly smaller than 180° do not prevent hydrogen bond formation, though their stabilizing contribution is significantly reduced (for a thorough discussion on this topic we refer the interested reader to Ref. [48]), and this is likely to be the case in **1**-Eta and **1**-Ets. The properties of H-bonds in these isomers are typical of closed-shell interactions; the electron density at the bcp is about one order of magnitude smaller than typical of the primary bonding structure ($\rho = 0.031$ and 0.027 e/Å^3 in **1**-Eta and **1**-Ets, respectively), while $\nabla^2(\rho)$ assumes positive values ($\nabla^2(\rho) = 0.120$ and 0.115 e/Å^5 in **1**-Eta and **1**-Ets, respectively). The DI between hydrogen and oxygen involved in H-bonding measures 0.075 and 0.062 in **1**-Eta and **1**-Ets, respectively (Table 6). These values are comparable to the DI (Cl, N–<u>H</u>) in **1**-Zta and **1**-Zts, suggesting that the O⋯H and Cl⋯H interactions concur to the energy stabilization with similar strength. The lower stability of **1**-Etγ isomers with respect to **1**-Ztγ can be rationalized considering that, in the former, the favorable dipolar interaction between N–H and C–Cl vanishes and is not fully compensated by the H-bond formation.

Another noticeable feature is that in **1**-Etγ the *anti* conformer is much more stable than the *syn* one, contrary to what was observed in **1**-Ztγ, **1**-Zcγ, and **1**-Ecγ pairs. A stabilizing contribution to the *anti* conformer comes from the O⋯H bond, which in **1**-Eta is shorter and stronger than in **1**-Ets. Secondly, in **1**-Ets, the electron density at the critical points of the C_{ipso}–N and the C=O bonds loses part of its shared character, with $-\nabla^2(\rho)$ at the bcp decreasing by 29% and 36% with respect to **1**-Eta, respectively. The loss of the covalent character of electrons partaking to these bonds—which comes from a subtle interplay of electronic effects involving resonant structures—further contributes to destabilizing **1**-Ets with respect to **1**-Eta.

The isomers **1**-Zca and **1**-Zcs reside at considerably higher energies with respect to the $\theta = t$ isomers considered so far. Indeed, in **1**-Zca and **1**-Zcs there are neither intermolecular hydrogen bonds nor favorable N–H/C–Cl dipolar interactions. Furthermore, the phenyl group rotates out of the molecular plane, inducing a noticeable rearrangement in the bonding structure. The C_{ipso}–N bond elongates and weakens; ρ at the bcp decreases by about 10% with respect to the more stable conformations discussed above, while a 5% decrease is observed in $-\nabla^2(\rho)$. The π character of this bond reduces as well, becoming more similar to a single bond. These same effects, and even more markedly, are observed in N–N, while the opposite happens in C=N. Overall, the delocalization of the π structure over the entire molecule is reduced, and π electrons localize mostly along the C=N internuclear axis. Overall, the two isomers, **1**-Zca and **1**-Zcs, share the same electronic structure. The relative energy ordering between the two is dictated by the dipolar interaction of C–Cl with C=O or C–O, analogous to the case of **1**-Zta and **1**-Zts. The lower stability of **1**-Zca with respect to **1**-Zcs comes therefore as no surprise.

As for the isomers at even higher energies, **1**-Eca and **1**-Ecs, the molecule becomes even less planar and the delocalization of π electrons further reduces, as indicated by the low ellipticity of ρ at all bcps except that of C=N. Noticeably, in the N–N bond, the shared character of electrons (measured by $-\nabla^2(\rho)$ at the bcp) reduces by about 10% with respect to **1**-Zca and **1**-Zcs, even if the internuclear distance and the net atomic charges remain unaltered. The isomer **1**-Eca is almost degenerate with **1**-Ecs, and the two share very similar electron density distributions. We just note that in **1**-Eca the ellipticity of the C–C bond is reduced with respect to **1**-Ecs (0.04 compared with 0.08), suggesting an even smaller delocalization of π electrons. The lower stability of **1**-Eca with respect to **1**-Ecs is probably due to this effect, together with a slightly larger steric hindrance between the methyl and phenyl groups.

In summary, our QTAIM analysis evidenced that in the planar, $\theta = t$ isomers of **1**, the π bonding structure is not independently localized onto the O=C–C=N chain of sp^2 atoms in the hydrazonic moiety and on the aryl ring, as assigned on the basis of chemical intuition. In particular, the N–N bond also has a partial but relevant π character, in agreement with

the analysis of the energetics and geometry of these isomers. Secondly, intramolecular hydrogen bonding between H and O occurs whenever these two atoms face each other (**1**-Etγ), as suggested by energetics and geometry. The QTAIM analysis enables us to trace the predominance of the *Z* isomers back to the electrostatic interaction between the C–Cl and N–H bond dipoles. Therefore, the energy ordering of the four planar isomers can be rationalized simply in terms of a balance between H-bond stabilization and dipole–dipole interactions. As for high energy isomers, their lower stability is mainly driven by the weakening of the delocalized π bonding structure.

3.1.5. Structure and Energetics of the Isomers of Halogen-Substituted Chlorohydrazone **2**–**7**

After the detailed analysis of the isomerism of **1**, we turn to the halogen-substituted chlorohydrazones **2**–**7**. The relative free energy of the isomers can be found in Tables S8–S13 (Supplementary Materials) and in Figure 11.
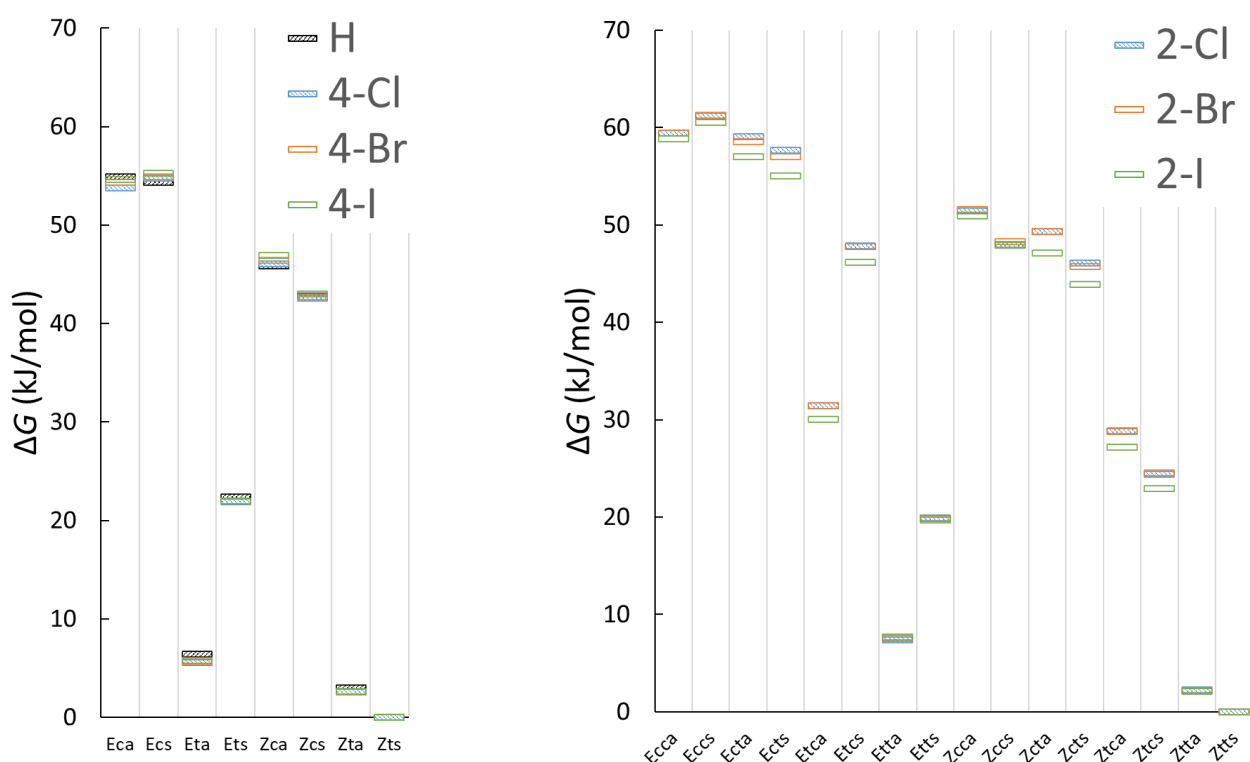

Figure 11. Relative free energy at 298 K of the minimum energy structures of **1**–**4** (**left**) and **5**–**7** (**right**) calculated at the ωB97M-D4/cc-pVTZ level. The vertical lines are just a guide for the eye.

The qualitative picture of the isomer energetic location is the same for all investigated chlorohydrazones **1**–**7**, so the previous qualitative analysis of **1** also applies to **2**–**7**. The ΔG between isomers changes by less than 5 kJ/mol upon halogen substitution.

The isomers of 4-X (X = Cl, Br, I) substituted chlorohydrazones **2**–**4** have structures and energetics very similar to those of the corresponding isomers of **1**. The calculated geometry of **3**-Zts is very close to that measured by XRD (Table 7). Clearly, the qualitative analysis is also the same as for **1**. The presence of the halogen in position 4 causes ΔG changes of a maximum of 1.1 kJ/mol. Then, the isomer energetics are scarcely influenced by the electronic availability in the aryl ring. The population of the three low-lying isomers varies by a few percent at most.

Table 7. Selected molecular geometric parameters of the Zts isomer of **3** calculated at the ωB97M-D4/cc-pVTZ level compared with those determined by XRD. Accuracy of the latter is shown in parentheses. Bond lengths are in angstrom, planar and dihedral angles are in degrees.

	C=N	N-N	N-C$_{ipso}$	Φ	θ	ψ	$\delta\Sigma$
Zts	1.268	1.311	1.393	121.13	179.95	179.79	0.0
XRD (Zts)	1.277(3)	1.329(2)	1.397(3)	120.02(18)	173.19(19)	178.1(2)	−0.6

$\delta\Sigma$ is the difference, $\delta\Sigma = 360° - \Sigma$, where Σ is the sum of the planar angles about the aminic N atom.

The general picture of the structure (Figure 12) and energetics (Figure 11, right) of the isomers of the 2-X substituted **5–7** are not much different from that of **1–4**, provided that the presence of a halogen atom in position 2 of the aryl ring is considered. The halogen may sterically and electrostatically interact with the rest of the molecule, and, at any rate, its mere presence gives rise to additional ψ isomerism (conformation about the N–Ar bond). Therefore, the chlorohydrazones **5–7** deserve a brief discussion.
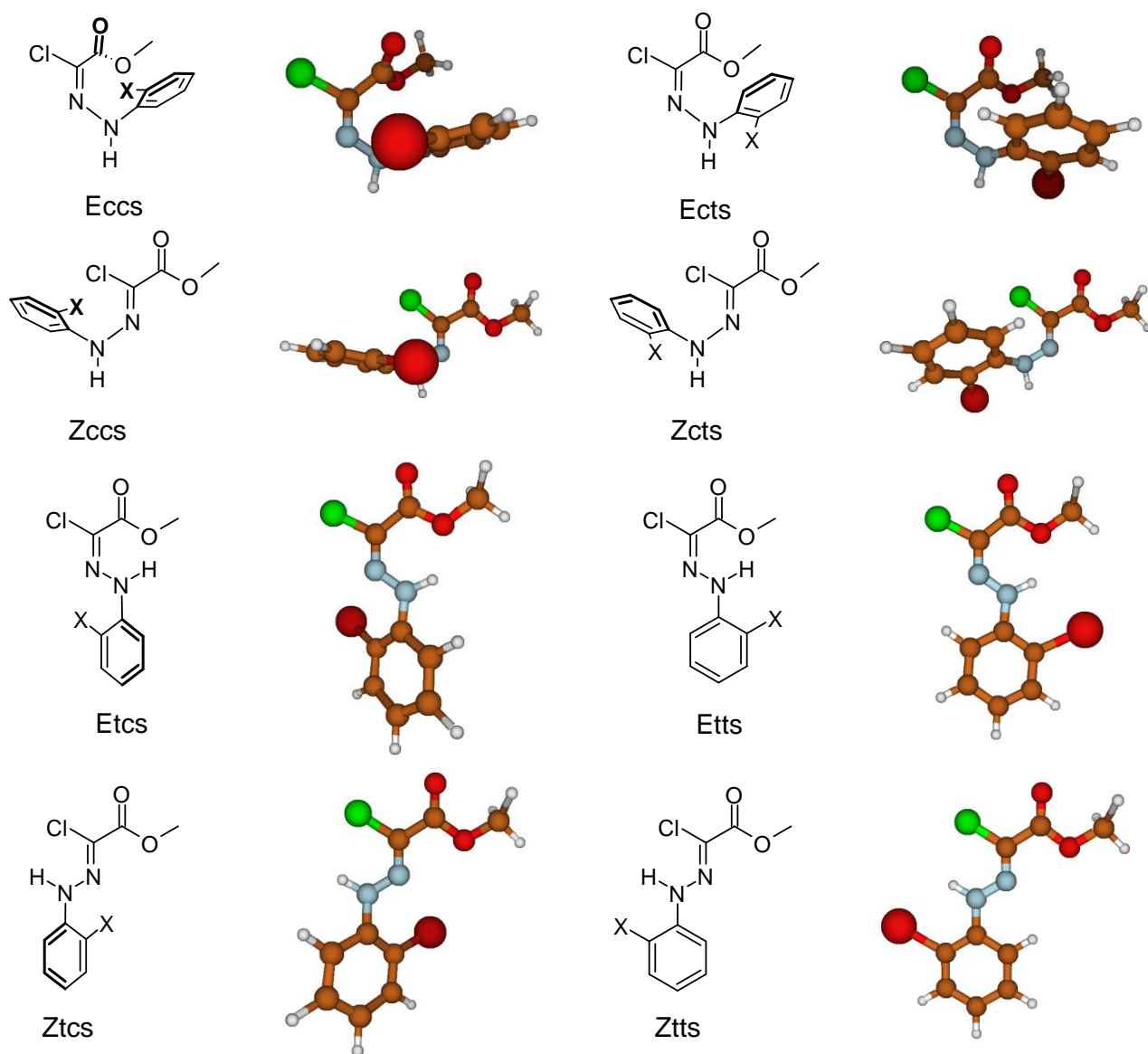

Figure 12. Selected (γ = s) ωB97M-D4/cc-pVTZ minimum energy structures of **7** (X = I). They are representative of the corresponding γ = a isomers and of the structures of **5** and **6**.

Among the **5**–**7** isomers, the planar ones are the (E,Z)ttγ; the other isomers have more or less extended but, in all cases, twisted conformations. The (E,Z)tcγ isomers are non-planar ($\psi \approx$ 49 to 58°) and thus are probably destabilized by the decreased conjugation between the aryl and hydrazone moieties, though they retain quasi-planar coordination around the –NH– nitrogen atom ($\delta\Sigma$ between 3 and 7°).

The θ = t [(**5**–**7**)-Φt$\psi\gamma$] isomers are more stable than the θ = c [(**5**–**7**)-Φc$\psi\gamma$] isomers by several tens of kJ/mol. This difference is larger for the ψ = t than the ψ = c isomers because the Φttγ are much lower in G than the Φtcγ isomers, whereas the Φctγ and Φccγ isomers have similar energy. This is probably due to the unfavorable location of the electron rich atoms Cl, iminic N, and X on the same molecular edge, which electrostatically repel and destabilize the Φtcγ with respect to the Φttγ isomers, a situation that does not occur in the twisted Φctγ and Φccγ isomers. The ψ = t [(**5**–**7**)-$\Phi\theta$tγ] isomers are in all cases more stable than the corresponding ψ = c [(**5**–**7**)-$\Phi\theta$cγ] isomers, but the free energy difference is much larger when θ = t.

The net result of these interactions is that the most stable isomers are the (**5**–**7**)-Φttγ. They lie 10–25 kJ/mol higher and the θ = c [(**5**–**7**)-Φc$\psi\gamma$] isomers are grouped together at $\approx$50 kJ/mol higher.

The H-bond stabilizes both (**5**–**7**)-Et(t,c)a isomers and the effect is weaker for the ψ = t ($\approx$10 kJ/mol) isomers than for the ψ = c ($\approx$16 kJ/mol). The latter value is in line with that of **1**–**4**. The lower value for ψ = t might be related to the electrostatic interaction between N–H and X, which competes with the N–H $\cdots$ O interaction.

The interplay between Φ, θ, ψ, and γ isomerisms is such that only three isomers of **5**–**7** are appreciably populated at 298 K, namely Ztts, Ztta, and Etta.

In this section, we have shown that the most stable isomer of investigated **1**–**7** systems is Zt(t)s, followed by the similar Zt(t)a. The Zt(t)γ isomers together account for >90% of the isomeric forms. Unexpectedly, the Et(t)a isomer is present only as a minor fraction of the isomeric forms, notwithstanding the N–H $\cdots$ O hydrogen bond. These planar isomers seem to have π conjugation extending to the whole molecular skeleton, which is transmitted through a planar tri-coordinated nitrogen atom.

3.2. Kinetics of the Isomerization of Chlorohydrazones **1**–**7**

3.2.1. Generalities

Several isomer interconversion processes can occur in chlorohydrazones **1**–**7** related to the (*E, Z*) isomers and the θ, ψ, and γ conformers (Figure 13). Conformational isomers can interconvert by rotation about the N–N (θ), C–COOMe (γ), and N–C_{ipso} (ψ) bond.

The number of isomerization processes is 12 for **1**–**4** and 32 for **5**–**7**. Since each isomerization proceeds through a TS, characterization of the isomerization dynamics of **1**–**7** requires locating 144 TSs. As a result of the large number of TSs, we conducted a thorough investigation of **1** at the ωB97M-D4/cc-pVTZ level while we restricted the investigation to the most significant TS structures in the **2**–**7** species. The TSs are denoted as **n**-$\Phi\theta\psi\gamma\Phi'\theta'\psi'\gamma'$.

3.2.2. Isomerization Transition States of Chlorohydrazone **1**

For the sake of clarity, we first discuss the isomer interconversion kinetics of **1**. The free energy activation barriers $\Delta G^{\ddagger}$ and the corresponding rate constants, calculated using the Eyring formula $k = \kappa \, (k_B T/h) \exp (-\Delta G^{\ddagger}/RT)$ with $\kappa = 1$ and $T = 298$ K, are collected in Table 8 and in Figure 14, grouped as to the interconversion process.
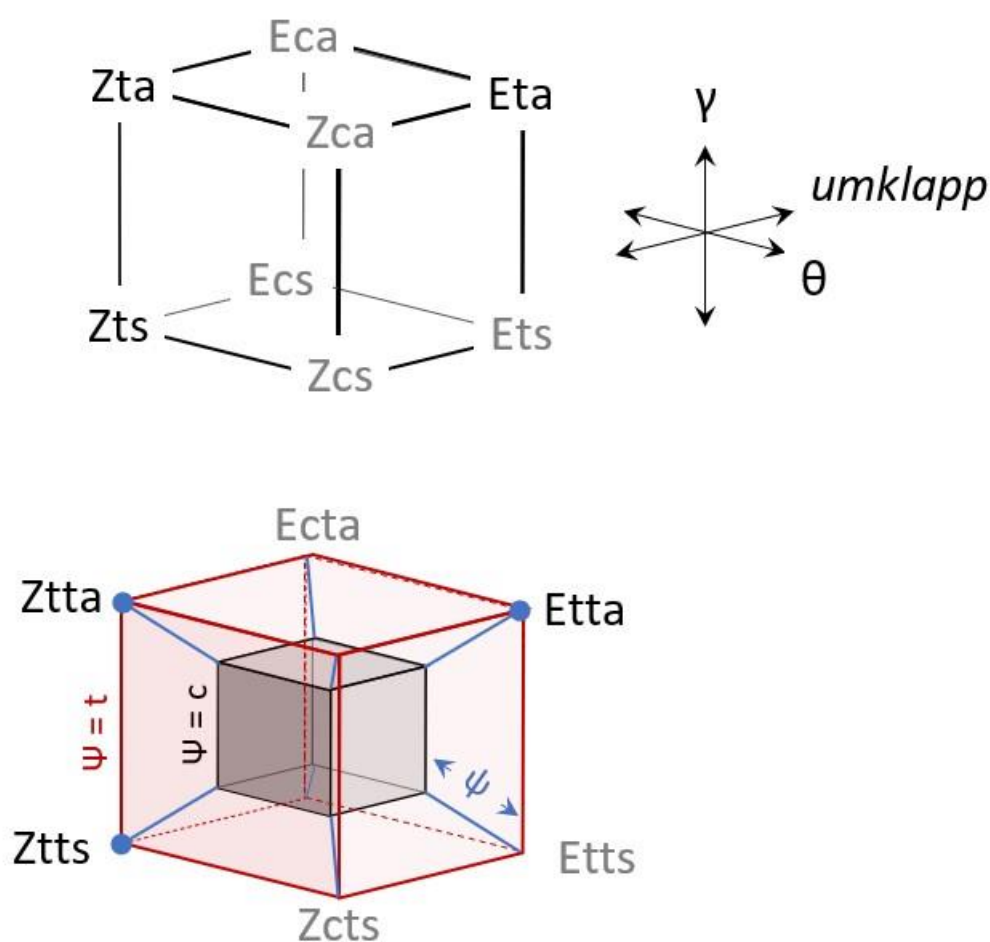
Figure 13. Schematic depiction of the isomer interconversion processes occurring in the chlorohydra-zones **1–7**. Top: interconversions of **1–4**. The eight isomers are placed at the vertices of a cube and the edges represent *umklapp*, θ, and γ interconversions. The non-populated isomers are grayed. Bottom: interconversions of **5–7**. The 16 isomers can be placed at the vertices of a sort of hypercube, the ψ = c and t isomers lie at the vertices of the inner black and outer red cubes, respectively. The important isomers Ztts, Ztta, and Etta are denoted by a blue dot. The blue lines are processes interconverting ψ isomers. Processes within the inner and outer cubes are as in the top panel.

Table 8. Free energy activation barriers, $\Delta G^{\ddagger}$, calculated at the ωB97M-D4/cc-pVTZ level, and corresponding rate constants at 298 K for the isomer interconversion processes of **1**. The barriers are grouped with respect to the interconversion mechanism.

Isomerization	From	To	$\Delta G^{\ddagger}$ (kJ/mol)	k (s^{-1}) [a]
	Eca	Ecs	7.4	$3.2 \cdot 10^{11}$
	Ecs	Eca	7.9	$2.6 \cdot 10^{11}$
	Eta	Ets	37.4	$1.7 \cdot 10^{6}$
Rotation,	Ets	Eta	21.4	$1.1 \cdot 10^{9}$
γ	Zca	Zcs	9.6	$1.3 \cdot 10^{11}$
	Zcs	Zca	12.7	$3.7 \cdot 10^{10}$
	Zta	Zts	19.5	$2.4 \cdot 10^{9}$
	Zts	Zta	22.5	$7.1 \cdot 10^{8}$

Table 8. *Cont.*

Isomerization	From	To	$\Delta G^{\ddagger}$ (kJ/mol)	k (s^{-1}) [a]
	Eca	Eta	27.3	$1.0 \cdot 10^8$
	Eta	Eca	75.8	0.33
	Ecs	Ets	27.8	$8.4 \cdot 10^7$
Rotation,	Ets	Ecs	59.7	$2.2 \cdot 10^2$
θ	Zca	Zta	20.8	$1.4 \cdot 10^9$
	Zta	Zca	63.7	43
	Zcs	Zts	18.8	$3.2 \cdot 10^9$
	Zts	Zcs	61.6	100
	Eca	Zta	59.8	210
	Zta	Eca	111.7	$1.6 \cdot 10^{-7}$
	Ecs	Zts	68.1	7.2
Umklapp, Φ (θ)	Zts	Ecs	122.5	$2.2 \cdot 10^{-9}$
	Eta	Zca	104.5	$3.1 \cdot 10^{-6}$
	Zca	Eta	65.0	25
	Ets	Zcs	89.9	$1.1 \cdot 10^{-3}$
	Zcs	Ets	69.6	4.0

[a] The rate constants were calculated using the Eyring formula $k = \kappa \, (k_B T/h) \exp(-\Delta G^{\ddagger}/RT)$ with $\kappa = 1$ and $T = 298$ K.
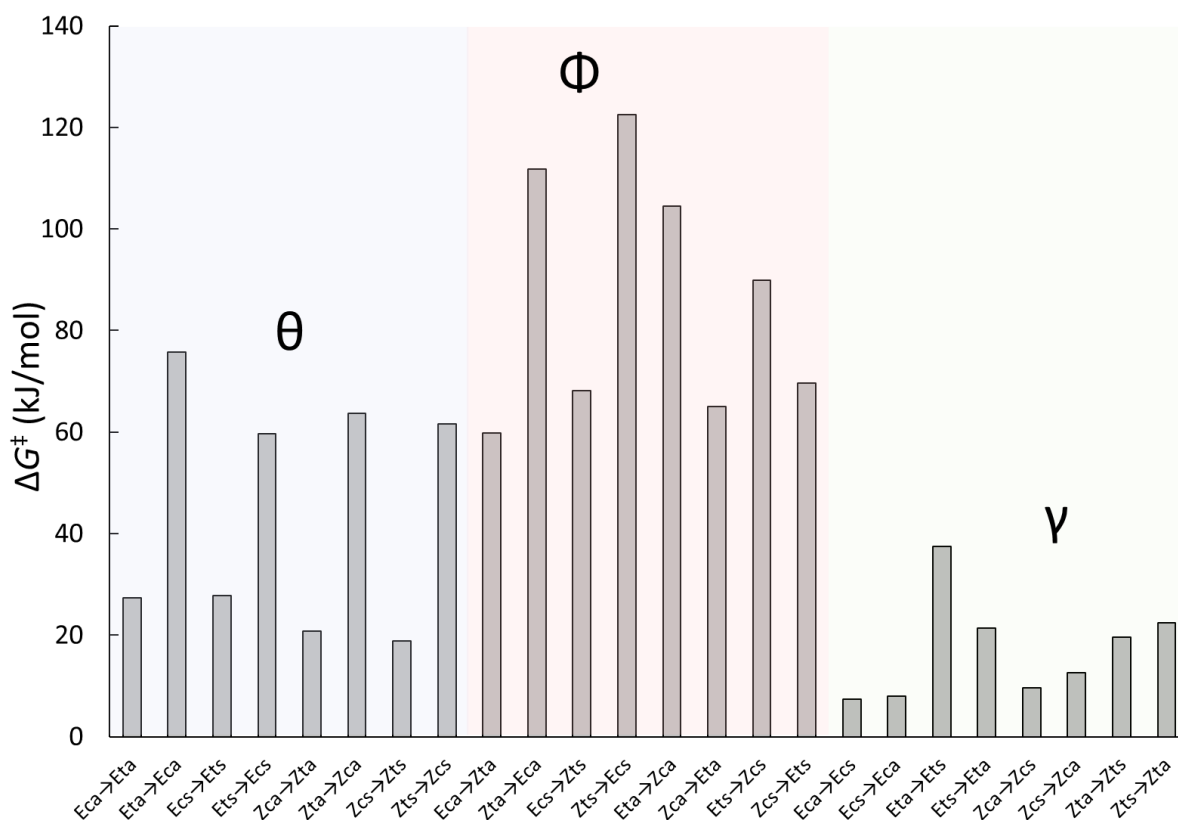

Figure 14. Activation barriers, $\Delta G^{\ddagger}$, at 298 K of the isomerization processes of **1** calculated at ωB97M-D4/cc-pVTZ level of theory. The barriers are grouped as to the isomerization type.

Selected TS structures are shown in Figure 15 and selected molecular geometric parameters of the TS structures of **1** are collected in Table 9.
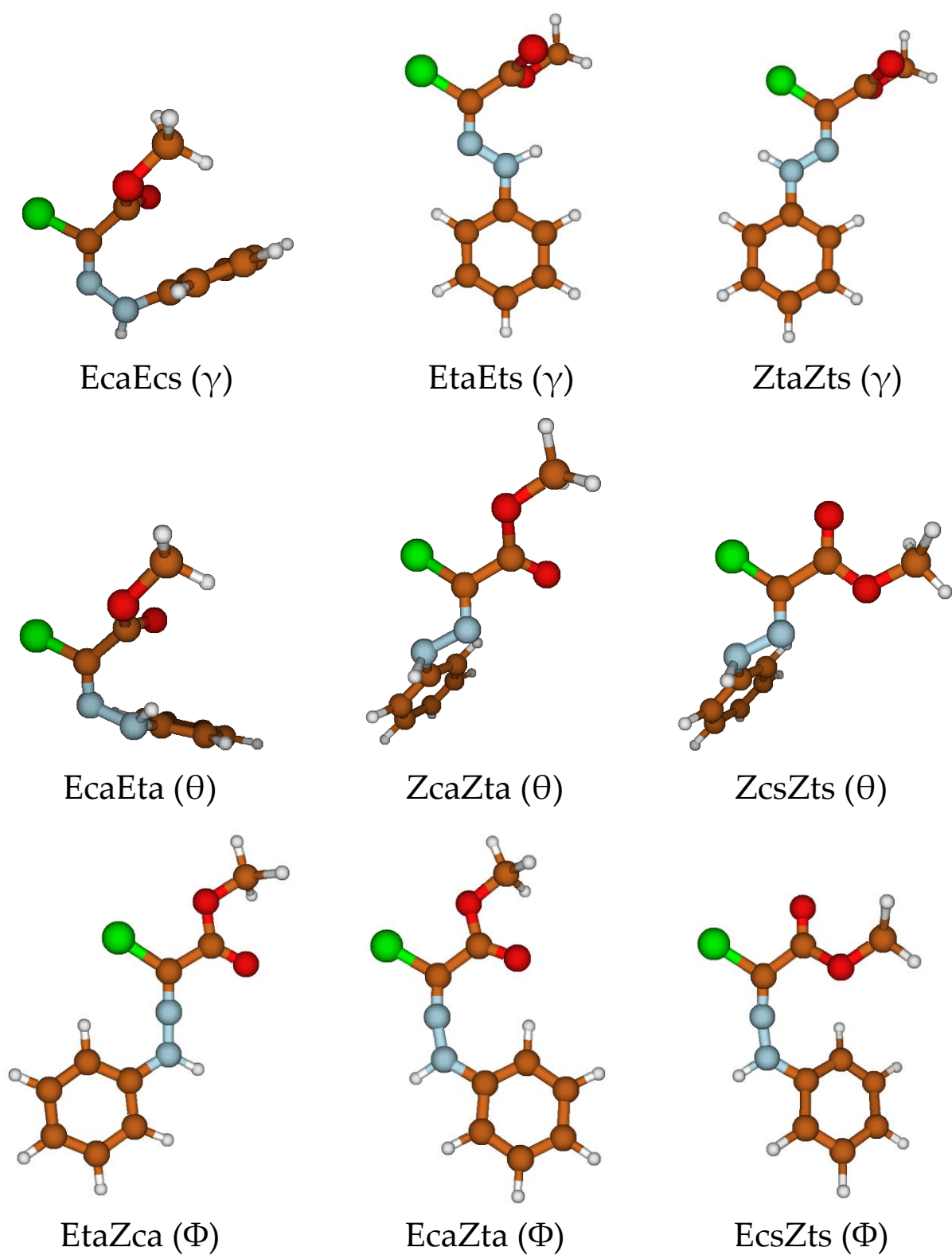
Figure 15. Selected transition state structures of **1** calculated at the ωB97M-D4/cc-pVTZ level. The process type is indicated in parentheses.

Table 9. Selected molecular geometric parameters of the TS structures of **1** calculated at the ωB97M-D4/cc-pVTZ level. Bond lengths are in angstroms, planar and dihedral angles are in degrees. When $\Phi \approx 180°$, θ is of limited structural meaning, as the C=N–N moiety is nearly linear.

Isomerization	TS	C=N	N-N	Φ	θ	ψ	$\delta\Sigma$
Rotation, γ	EcaEcs	1.259	1.346	235.5	0.0	−113.4	2.6
	EtaEts	1.259	1.347	240.3	170.4	16.3	5.5
	ZcaZcs	1.254	1.382	120.1	−64.7	−7.9	23.4
	ZtaZts	1.257	1.332	121.2	175.3	9.5	1.1
Rotation, θ	EcaEta	1.257	1.436	243.6	−54.1	−34.6	18.4
	EcsEts	1.258	1.436	243.6	−54.8	−33.0	18.5
	ZcaZta	1.252	1.428	115.6	121.0	−31.4	31.4
	ZcsZts	1.256	1.427	115.3	118.8	−25.5	31.1
Umklapp, Φ (θ)	EcaZta	1.225	1.281	191.0	0.9	−1.9	0.1
	EcsZts	1.222	1.282	187.5	−17.5	−19.1	0.4
	EtaZca	1.220	1.276	179.8	−30.7	1.1	0.0
	EtsZcs	1.220	1.276	179.1	163.2	1.1	0.0

$\delta\Sigma$ is the difference, $\delta\Sigma = 360° - \Sigma$, where Σ is the sum of the planar angles about the –NH– atom.

The interconversion between the γ = (a, s) conformers is trivial. The barriers are generally low since no covalent bond is broken. Even when a hydrogen bond is broken during the interconversion of the **1**-Et(a,s) pair, the rate constants at 298 K are very high. Thermal equilibrium within each **1**-$\Phi\theta$(a,s) pair is thus expected to be established quickly at 298 K. The TS structures are characterized by an angle between the COOMe group and the Cl–C=N fragment close to 90°, even in the crowded TS between **1**-Eca and **1**-Ecs.

The interconversion between the θ = (c, t) isomers occurs by rotation about the N–N bond. This isomerization occurs between isomer pairs separated by several tens of kJ/mol (Table 2) so the forward and backward barriers are largely different. We focus on the barriers from the more stable θ = t isomer to the θ = c isomer. These barriers are in the 60–75 kJ/mol range and the calculated rate constants are around 10^2 s^{-1}, except for the slower process between the high-lying **1**-Eta and **1**-Eca isomers. The isomerizations from θ = t isomers are many orders of magnitude slower than the γ isomerizations but it does not seem that the isomers can be separated, though the θ processes might be spectroscopically observed, e.g., by NMR. The TSs for the θ isomerization are characterized by an enhanced pyramidal character of the –NH– nitrogen atom (Table 8). For instance, $\delta\Sigma$ is about 30° for the **1**-ZcγZtγ TSs between planar **1**-Ztγ and **1**-Zcγ, which has a $\delta\Sigma$ well below 20°. Furthermore, we observe a dramatic elongation of the N–N bond from 1.31–1.35 Å in the minimum energy structures to 1.42–1.43 Å in the corresponding TSs. This process is clearly accompanied by a marked decrease in the sp^2 character of the –NH– nitrogen atom and disruption of the conjugation between the phenyl ring and the hydrazonic moiety.

We are particularly interested in the kinetics of the chemically important interconversion between the (*E*, *Z*) geometrical isomers. This has been briefly studied in the framework of substituted imines R^{1}R^{2}C = NR^3, including a few imines with heteroatoms on the N atom, such as oximes and hydrazones [49–51]. In the latter, (*E*, *Z*) geometrical isomerization occurs by the *umklapp* mechanism; for hydrazones (R^3 = NHR), the –NHR fragment rotates in the molecular plane towards a linear C=N–N configuration (which is usually close to the TS) and then proceeds to the other isomer (Figure 16, top). (*E*, *Z*) interconversion of hydrazones by rotation about the C=N bond (such as in ethylenes) does not. Our calculations confirmed this finding: we found *umklapp* TSs for **1**–**7** but, despite several attempts, TSs for the ethylene-like rotation about the C=N bond were not located.
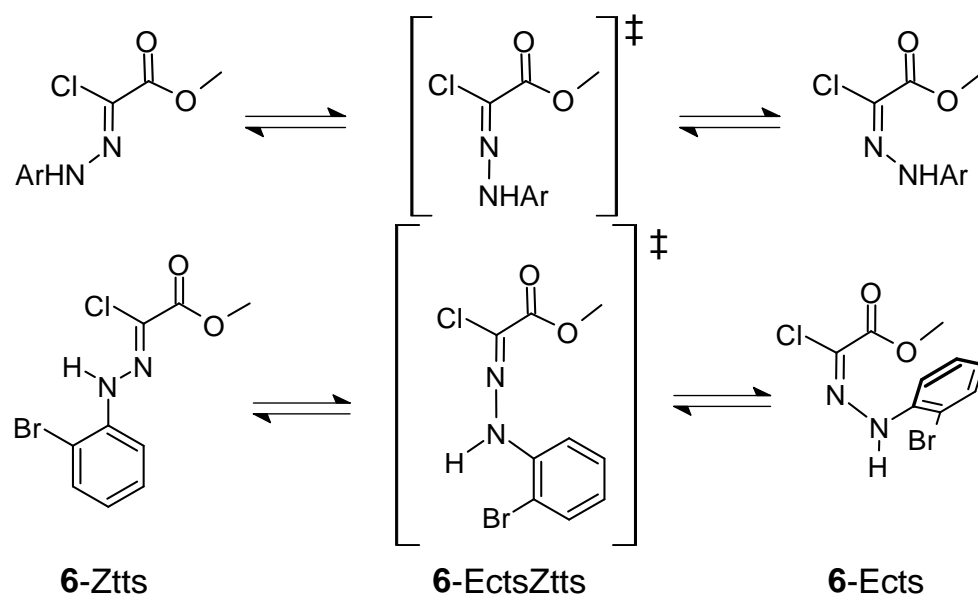
Figure 16. Schematic depiction of the *umklapp* mechanism for the (*E*, *Z*) interconversion in a generic *C*-methoxycarbonyl-*N*-aryl chlorohydrazone (**top**) and in the specific example **6**-Ztts/**6**-Ects (**bottom**).

Note that the *umklapp* mechanism for the (*E*, *Z*) interconversion involves an interconversion of the θ = (c, t) isomers, as can be appreciated by inspecting the example in Figure 16, bottom. Therefore, there is no direct interconversion between the important isomers Zt(t)a and Et(t)a; the *umklapp* step must be preceded (or followed) by at least one rotation about the N–N bond, i.e., an interconversion of the θ = (c, t) isomers. The (*E*, *Z*) interconversion between Zt(t)a and Et(t)a thus necessarily involves at least one of the high-energy isomers.

Umklapp occurs between isomer pairs separated by tens of kJ/mol (Table 2) so the forward and backward barriers are largely different also in this case. The barriers from the populated **1**-Ztγ and **1**-Eta isomer are in the 105–125 kJ/mol range (Table 7), sufficient to prevent isomerization at room temperature and enable isomer isolation. The calculated rate constants are many orders of magnitude smaller than those of θ isomerizations starting from θ = t isomers. The *umklapp* barrier is much lower than the internal rotation barrier of ethene (≈280 kJ/mol) [52]. Thus, the *umklapp* mechanism reasonably has a lower barrier for the (*E*, *Z*) isomerization than the putative internal rotation about the C=N bond as it does not involve breaking a covalent bond. However, *umklapp* barriers are too high (*E*, *Z*) to make the isomerization for C=N bonds thermally accessible.

All *umklapp* TSs have planar coordination about the –NH– nitrogen atom (Figure 15). The **1**-EtγZcγ TSs have an extended, planar structure with a linear C=N–N fragment (Table 8). This conformation is slightly perturbed in **1**-EcγZtγ TSs because of the steric hindrance between the phenyl ring and the COOMe group. This unfavorable interaction structurally affects **1**-EcsZts (ψ ≈ –17°) more than **1**-EcaZta (ψ ≈ 1–2°) and is probably also responsible for the slightly bent conformation of the C=N–N core (ca. 10°). A surprising peculiarity is found when analyzing the C=N and N–N bond lengths of the *umklapp* TSs (Table 8). The former is ≈1.22 Å long, about 0.5 Å shorter than in the minimum energy structures (Table 3). The N–N bond is ≈1.28 Å long in the *umklapp* TSs and 1.31 (1.34) Å in the minimum energy structures of the θ = t (c) isomers. Thus, the length of both bonds directly involved in the *umklapp* process are shorter in the TS than in the minimum energy structure. In the TSs, the N–N bond is slightly longer than the N=N distance in (phenyl)diazenes (Table 4). It may seem that the TS N–N bond is almost a double bond. Thus, in the *umklapp* TSs we find an increase in the bond order within the C=N–N fragment, which is the hotspot of the isomerization process. This is accompanied by a slight (≈0.1 Å) increase in the N–C_ipso length.

3.2.3. *Umklapp* Kinetics of Chlorohydrazone **1**

As we have seen, at 298 K the populated isomers are **1**-Zts, **1**-Zta, and **1**-Eta. The **1**-Zt(a,s) can be considered in thermal equilibrium on the timescale of the Φ and θ isomerization processes. Therefore, for the present we consider the interconversion between **1**-Zta and **1**-Eta, which cannot occur in a single step (Figure 16). The shortest paths are **1**-Zta $\rightleftharpoons$ **1**-Zca $\rightleftharpoons$ **1**-Eta and **1**-Zta $\rightleftharpoons$ **1**-Eca $\rightleftharpoons$ **1**-Eta. The energetics of these processes are shown in Figure 17. Consideration of the law of consecutive first-order reactions [53] shows that the **1**-Zta $\rightarrow$ **1**-Zca $\rightarrow$ **1**-Eta path (red arrows in Figure 17) is much faster than **1**-Zta $\rightarrow$ **1**-Eca $\rightarrow$ **1**-Eta because of the presence in the latter of the high **1**-Zta $\rightarrow$ **1**-Eca barrier. Similarly, path **1**-Eta $\rightarrow$ **1**-Eca $\rightarrow$ **1**-Zta (blue arrows in Figure 17) is much faster than that proceeding via **1**-Zca. Therefore, the **1**-Zta $\rightarrow$ **1**-Eta interconversion, and its inverse **1**-Eta $\rightarrow$ **1**-Zta, occur along different pathways and involve different intermediates.
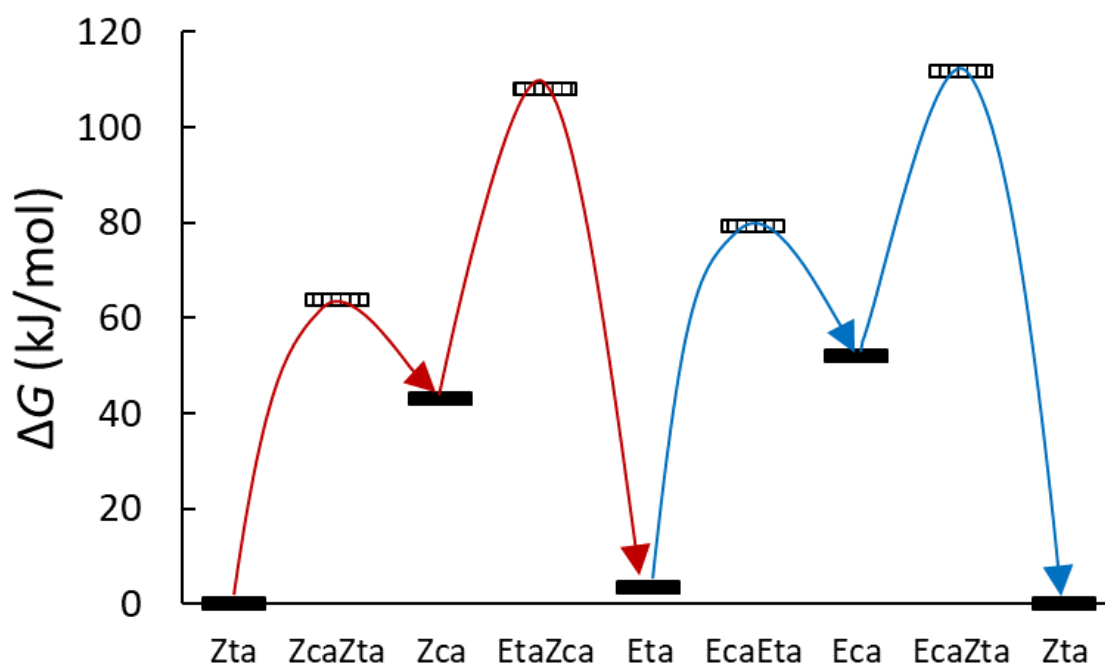

Figure 17. Energetics of the shortest paths for the interconversion between **1**-Zta and **1**-Eta comprising an *umklapp* (Φ) and a θ isomerization step. Solid bars indicate minimum energy isomers and hatched bars indicate transition states. The fast pathways are indicated by curved arrows.

There are, of course, many other paths involving more than one intermediate isomer. The whole kinetic network (Figure 13) is described by a system of first-order differential equations. The solution of the system allows one to calculate the isomer population kinetics and the velocity of any reactive path interconverting two given isomers. The well-known exponential matrix method is easily applied to our case, but it unfortunately turns out that the kinetic matrix is ill-conditioned, and the solution is numerically unstable. We therefore resort to a kinetic Monte Carlo (KMC) approach [41]. Due to the huge difference among the rate constants of the kinetic isomerization network (about 20 orders of magnitude) we were forced to assume that (a,s) pairs with significant population equilibrate much faster than Φ and θ interconversion processes. KMC simulations (Figure 18) clearly indicate that **1**-Zt(a,s) $\rightarrow$ **1**-Zc(a,s) $\rightarrow$ **1**-Et(a,s) and **1**-Et(a,s) $\rightarrow$ **1**-Ec(a,s) $\rightarrow$ **1**-Zt(a,s) processes dominate the dynamics of the interconversion among the populated isomers.

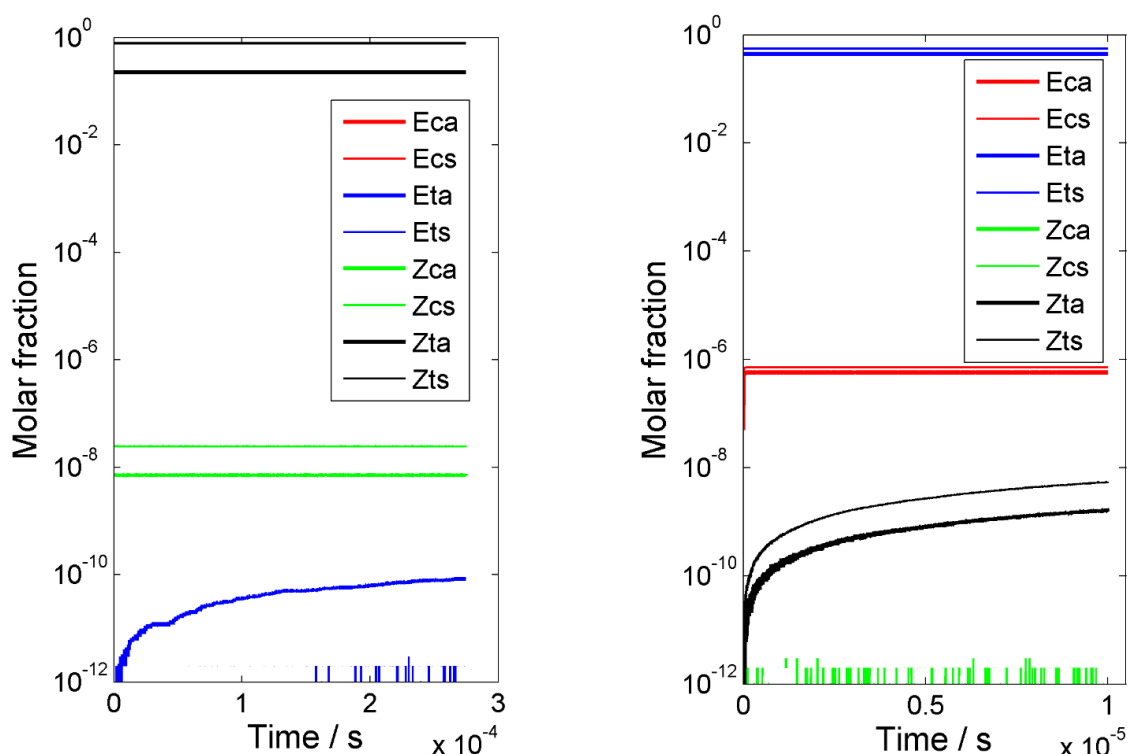**Figure 18.** Kinetic Monte Carlo simulations of the **1**-Zt(a,s) → **1**-Et(a,s) (**left**) and **1**-Et(a,s) → **1**-Zt(a,s) (**right**). The molar fraction of each isomer is plotted as a function of time.

In the KMC simulation starting from an equilibrium mixture of **1**-Zt(a,s) (Figure 18, left), **1**-Zc(a,s) is first formed. The timescale of the Figure is such that only the stationary-state concentration of **1**-Zc(a,s) is visible. After ≈10^{-5} s, an increasing population of **1**-Eta develops (the molar fraction of **1**-Ets is very small in the simulation time window). The simulation shows that the dynamics of the **1**-Zt(a,s) → **1**-Eta interconversion are dominated by the process occurring via **1**-Zcγ. By a similar reasoning, based on the KMC simulation starting from an equilibrium mixture of **1**-Et(a,s) (Figure 18, right), we find that **1**-Et(a,s) → **1**-Zt(a,s) is dominated by the process occurring via **1**-Ecγ. Therefore, also when all possible reactive paths are considered, the latter interconversion and its inverse occur by different mechanisms involving different intermediates.

3.2.4. Electronic Structure and π Delocalization of the *Umklapp* TSs of Chlorohydrazone **1**

The quasi-double bond nature of the N–N bond has no simple justification based on Lewis structures, since predominance of a charge-separated Lewis structure is unlikely. The ωB97M-D4/cc-pVTZ π MOs of **1**-EtsZcs (Figure S10) do not suggest stronger conjugation nor higher bond orders.

More detailed information about this issue will be provided by the following QTAIM bond analysis, carried out according to the same scheme adopted for stable isomers. The discussion is based on the QTAIM atomic and bond properties of the *umklapp* TSs of **1**, which are collected in Tables S1 and S2 in the Supplementary Materials along with the relevant bond lengths. As extensively described above, the most noticeable feature of these TSs is the almost linear N–N=C alignment, with N–N and C=N internuclear distances significantly shorter than those of the stable isomers connected by the TS (Tables 3 and 8). On the contrary, the C–Cl distances are elongated by more than 0.05 Å, and a smaller but non-negligible elongation of the (N=)C–COOMe internuclear distance occurs (Table S2). As for the electron density distribution, we first note that in stable isomers the two nitrogen atoms have similar atomic charges (about –0.7 e), while in the TSs they are significantly unbalanced. Indeed, the aminic nitrogen atom loses electrons and has a net charge of about

–0.6 e, while the iminic N gains electrons and reaches q = –0.9 e (Table S1). As for the iminic carbon atom, its positive charge increases from about +0.8 e in stable isomers to almost +0.9 e in the TSs. Chlorine also increased its excess electron population, from about –0.2 e to –0.3 e. These data suggest that resonant structures inducing positive charges on the aminic nitrogen and the iminic carbon and a negative charge on the iminic nitrogen are favored in the transition state with respect to the stable isomers. At the same time, the lone pairs of chlorine are less involved in bonding.

In addition, the variation of the bonding properties is mostly relevant along the N–N=C fragment (Table S2). The π character of the N–N bond is larger in the TS than the stable isomers; the electron density at the bcp increases from 5% to 15%, depending on the structures considered. The negative of the Laplacian increases as well, from 10% to almost 30%. The shortening of the N-N internuclear separation indeed corresponds to an increase in the shared character of the interaction, which gets closer to double-bonding between nitrogen atoms.

As for the C=N bond, which shortens, we did not find net features of a triple bond. In the TSs there is no further accumulation of electron density at the bcp with respect to the stable isomers. Furthermore, the positive curvature of the Hessian of ρ at the bcp becomes dominant over the two negative ones, leading to a positive value for the Laplacian at the bcp, which is typical of interactions dominated by charge separation instead of pure covalent bonds. This same conclusion can be drawn from trends in ellipticity at the C=N bond critical points. Indeed, ε is only slightly smaller with respect to stable isomers, while it should vanish in a triple bond. These data suggest only a residual triple bond character for C=N.

Overall, in transition states the charge separation between atoms is favored with respect to the stable isomers. The π conjugation due to the participation in bonding of the lone pairs of chlorine and oxygen atoms is reduced. The data indicate an increased partial double bond character for N-N, while no triple bond character emerges in C=N.

3.2.5. Isomerization Transition States of Chlorohydrazones **2–7**

After the detailed analysis of the isomerization TSs and kinetics of **1**, we turn to the halogen substituted chlorohydrazones **2–7**. For 4-X (X = Cl, Br, I)-substituted chlorohydrazones **2–4**, we optimized the four TSs involved in the just discussed interconversion between Zta and Eta, and the TS for the γ isomerization of the Zt(a,s) pair. In the case of the 2-X-substituted chlorohydrazones **5–7**, in addition to these five TSs (calculated for the more stable ψ = t case), we optimized the three TSs connecting the populated (**5–7**) Zttγ and (**5–7**) Etta isomers with their ψ = c counterparts.

The ωB97M-D4/cc-pVTZ free energy isomerization barriers corresponding to the selected TSs can be found in Tables 10 and 11 and in Figure 19.

Table 10. Free energy activation barriers, $\Delta G^{\ddagger}$, calculated at the ωB97M-D4/cc-pVTZ level, and corresponding rate constants at 298 K for selected isomer interconversion processes of **2–4**. The barriers are grouped with respect to the interconversion mechanism.

Isomerization	From	To	$\Delta G^{\ddagger}$ (kJ/mol)		
			2	**3**	**4**
Rotation,	Zta	Zts	19.4	18.9	18.8
γ	Zts	Zta	22.0	21.5	21.4
	Eca	Eta	22.7	22.0	21.5
Rotation,	Eta	Eca	70.9	70.7	70.2
θ	Zca	Zta	16.2	16.1	18.6
	Zta	Zca	59.7	59.9	62.9
	Eca	Zta	60.8	60.6	61.0
Umklapp, Φ	Zta	Eca	112.0	112.4	112.9
(θ)	Eta	Zca	105.9	106.0	106.1
	Zca	Eta	65.4	65.3	65.0

Table 11. Free energy activation barriers, $\Delta G^{\ddagger}$, calculated at the ωB97M-D4/cc-pVTZ level, and corresponding rate constants at 298 K for selected isomer interconversion processes of **5–7**. The barriers are grouped with respect to the interconversion mechanism.

Isomerization	From	To	$\Delta G^{\ddagger}$ (kJ/mol)		
			5	**6**	**7**
Rotation, γ	Ztta	Ztts	18.9	18.8	18.5
	Ztts	Ztta	21.2	21.0	20.6
Rotation, θ	Ecta	Etta	17.3	17.6	19.0
	Etta	Ecta	68.9	68.7	68.3
	Zcta	Ztta	10.4	10.4	16.9
	Ztta	Zcta	57.4	57.6	61.8
Rotation, ψ	Etca	Etta	6.1	5.9	5.8
	Etta	Etca	68.9	68.7	68.3
	Ztca	Ztta	5.0	5.2	5.5
	Ztta	Ztca	31.7	31.8	30.6
	Ztcs	Ztts	5.4	5.4	6.3
	Ztts	Ztcs	29.9	29.9	29.2
Umklapp, Φ (θ)	Ecta	Ztta	57.8	58.7	59.8
	Ztta	Ecta	114.6	115.1	114.7
	Etta	Zcta	104.9	104.6	104.2
	Zcta	Etta	63.0	62.8	64.8

The qualitative picture of the TS energetic location is the same for all investigated chlorohydrazones **1–7**, so the previous kinetic analysis of **1** also applies to **2–7**.

The TSs of 4-X (X = Cl, Br, I)-substituted chlorohydrazones **2–4** have structures very similar to those of the corresponding TSs of **1**. Upon halogen substitution in position 4, the change in $\Delta G^{\ddagger}$ barrier is ≈5–7 kJ/mol for θ isomerizations, <5 kJ/mol for Φ processes, and a few kJ/mol for γ isomerizations (Table 10 and Figure 19, top). Similar to the minimum energy structures, the TS energetics are scarcely influenced by the electronic availability in the aryl ring. The differences between **2–4** are generally small (<2 kJ/mol). The barriers to the Zta ⇌ Eca isomerization increase from Cl < Br < I, whereas those of the Zca ⇌ Eta isomerization decrease in the same direction. The barrier difference is somewhat larger for θ isomerizations.

The general picture of the TS structures (Figure 20) and associated barriers (Table 11 and Figure 19, bottom) of the 2-X-substituted **5–7** are not much different from that of **1–4**, provided that the presence of a halogen atom in position 2 of the aryl ring is considered. The halogen may sterically (and electrostatically) interact with the rest of the molecule; however, its mere presence give rise to the additional ψ isomerism (conformation about the N-Ar bond). Therefore, the TSs of chlorohydrazones **5–7** deserve some discussion. The barriers of the Φ and γ isomerizations are very similar across the whole **1–7** set because the possible steric hindrance introduced by the halogen in position 2 is found in the more extended conformation of the Φ TSs and is nearly constant in the γ TSs. The *umklapp* barriers of **5–7** are either slightly lower or higher than those of **1**. No clearcut trend can be seen when comparing the *umklapp* barriers of **5–7**. Somewhat larger differences can be seen in the θ TSs, e.g., for the Zcta to Ztta isomerization. The ψ barriers related to the populated isomers are highly asymmetric. In the corresponding TSs, the aryl ring is approximately perpendicular to the hydrazonic moiety (ψ ≈ 65° (opposite to NH) for ZtcaZtta and ZtcsZtts, ψ ≈ 74° (towards NH) for EtcaEtta). The barriers related to the Zttγ isomers (≈30 kJ/mol) are low enough for fast equilibration at RT. The Etta → Etca barrier is much higher (≈69 kJ/mol) and could lead to observable effects.

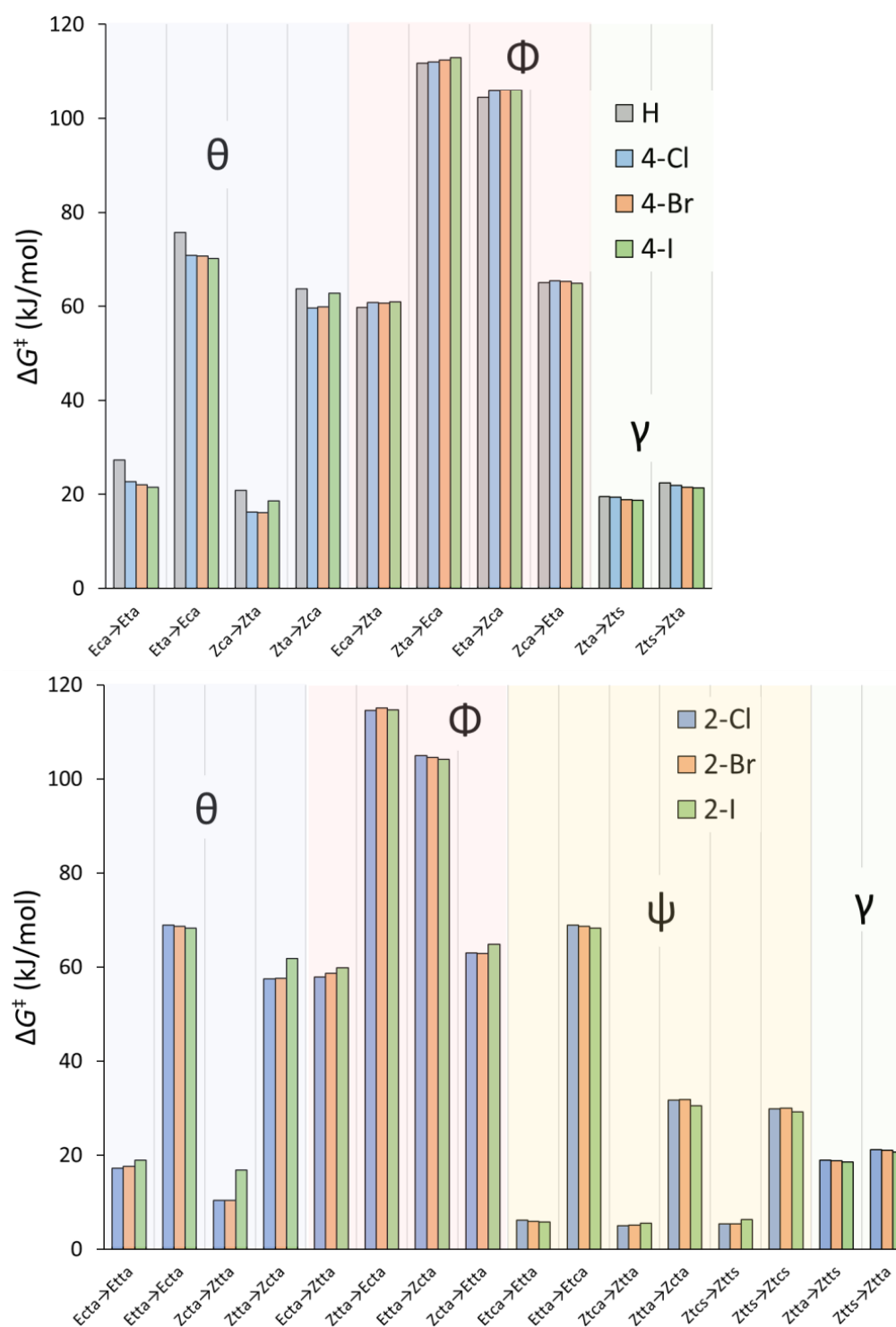**Figure 19.** Activation barriers, $\Delta G^{\ddagger}$, of the isomerization processes of **1**–**7** at 298 K, calculated at the ωB97M-D4/cc-pVTZ level of theory. The barriers are grouped as to the isomerization type. The vertical lines are just a guide for the eye.
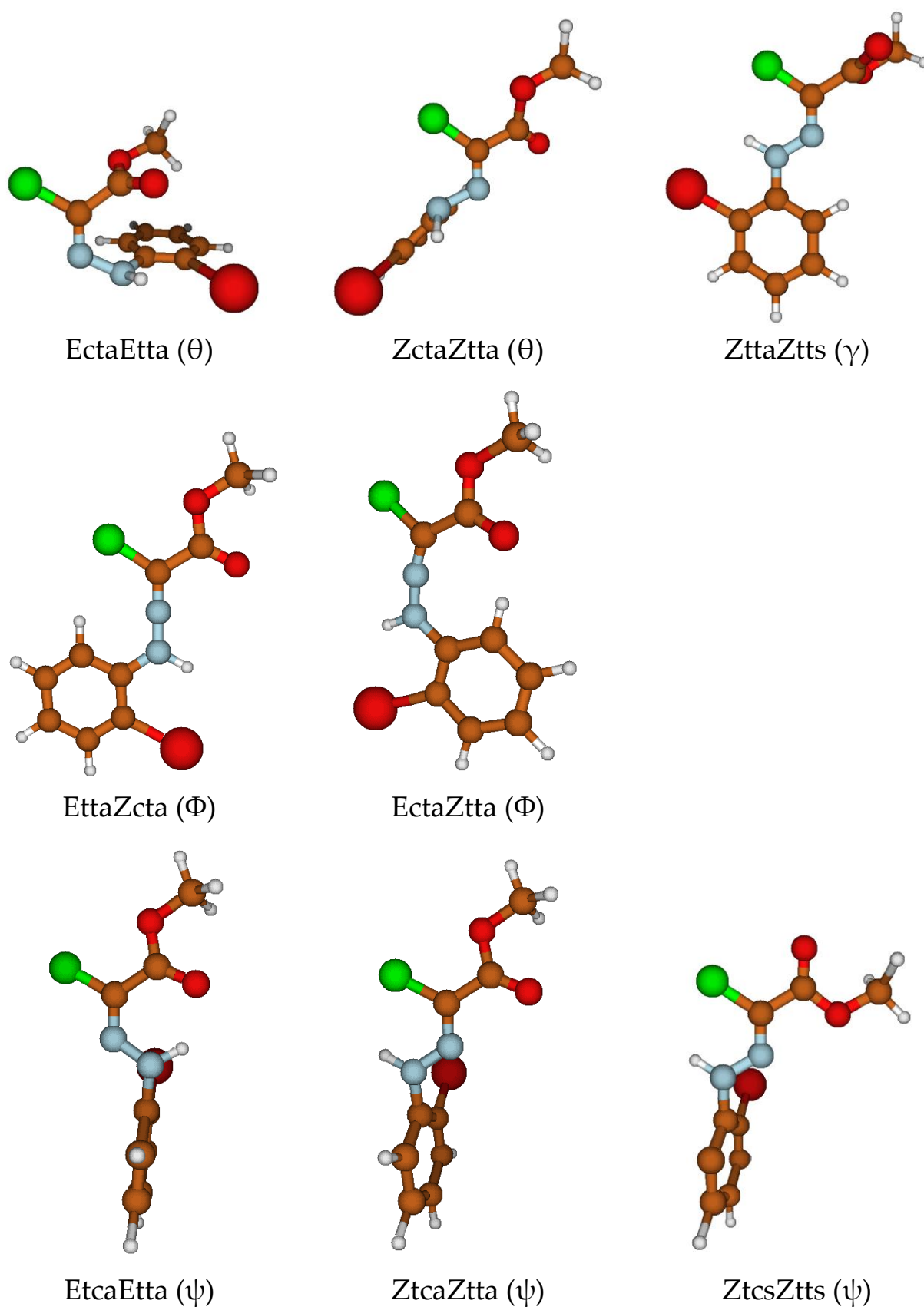
Figure 20. Selected transition state structures of **7** calculated at the ωB97M-D4/cc-pVTZ level. The process type is indicated in parentheses. They are representative of the corresponding transition state structures of **5** and **6**.

4. Conclusions

Analysis of the electron density, energetics, and structure of the isomers of *C*-methoxycarbonyl-*N*-aryl chlorohydrazones **1–7** calculated at the ωB97M-D4/cc-pVTZ level of theory, supported by the XRD determination of the molecular structure of **1** and **3**, allowed us to answer the three questions we posed in the Introduction. Isomers with a transoid configuration about the N–N bond are planar and feature a molecule-wide delocalization of π electrons occurring over a formally sp^3 nitrogen atom. Within these low-energy planar isomers, the *Z* isomers are thermodynamically favored because the favorable electrostatic interactions between the dipoles of the C–O, C–Cl, and N–H bonds overcome the stabilization induced by the real N–H $\cdots$ O hydrogen bond present in the *E* isomers. The prevalence of *E* or *Z* is a delicate balance of interactions that can be modulated by changing the substituents on the iminic carbon. The (*E*, *Z*) isomerization is very slow at room temperature because the interconversion among the low-energy planar isomers involves the *umklapp* interconversion that has high barriers (≈110 kJ/mol) despite the extended electron delocalization present in the TS. We note that the (*E*, *Z*) isomerization is a two-step process involving one *umklapp* and one θ (N–N rotation) interconversion.

References

1. Fisher, E. Uber Die Hydrazinwerbindung. *Liebigs Ann.* **1882**, *212*, 316. [CrossRef]
2. Ulrich, H. *The Chemistry of Imidoyl Halides*; Plenum Press: New York, NY, USA, 1968.
3. Shawali, A.S.; Párkanyi, C. Hydrazidoyl halides in the synthesis of heterocycles. *J. Heterocycl. Chem.* **1980**, *17*, 833–854. [CrossRef]
4. Shawali, A.S. Reactions of heterocyclic compounds with nitrilimines and their precursors. *Chem. Rev.* **1993**, *93*, 2731–2777. [CrossRef]
5. Shawali, A.S.; Abdallah, M.A. The chemistry of heterocyclic hydrazonoyl halides. In *Advances in Heterocyclic Chemistry*; Elsevier: Amsterdam, The Netherlands, 1995; Volume 63, pp. 277–338. [CrossRef]
6. Shawali, A.S.; Mosselhi, M.A.N. Hydrazonoyl halides: Useful building blocks for the synthesis of arylazoheterocycles. *J. Heterocycl. Chem.* **2003**, *40*, 725–746. [CrossRef]
7. Shawali, A.S. A Review on bis-hydrazonoyl halides: Recent advances in their synthesis and their diverse synthetic applications leading to bis-heterocycles of biological interest. *J. Adv. Res.* **2016**, *7*, 873–907. [CrossRef] [PubMed]
8. Donohue, S.R.; Halldin, C.; Pike, V.W. A facile and regioselective synthesis of rimonabant through an enamine-directed 1,3-dipolar cycloaddition. *Tetrahedron Lett.* **2008**, *49*, 2789–2791. [CrossRef]
9. Shawali, A.S. Hydrazonoyl halides: A bubbling fountain of biologically active compounds. *Curr. Org. Chem.* **2010**, *14*, 784–815. [CrossRef]

10. Moon, M.W.; Friedman, A.R.; Steinhards, A. Herbicidal activity of phenylhydrazones and related azo compounds. *J. Agric. Food Chem.* **1972**, *20*, 1187–1190. [CrossRef]

11. Kukota, S.N.; Borisenko, V.P.; Bodnar, V.N.; Zhuravskaya, N.I.; Lozinskii, M.O. Syntehsis and phytotoxicity of arylhydrazones of substituted pyruvic and a,ß-dioxobutyric acids. *Fiziol. Akt. Veshchestva* **1978**, *10*, 32–36.

12. Moore, J.E. Insecticidal Phenylhydrazone Sulfides. U.S. Patent 3,932,660, 13 January 1976.

13. Folz, S.D.; Pax, R.A.; Klei, T.R.; Thomas, E.M.; Ash, K.A.; Conder, G.A.; Bennett, J.L. Development of a novel in vitro equine anthelmintic assay. *J. Vet. Pharmacol. Ther.* **1988**, *11*, 177–182.

14. Molodykh, Z.V.; Buzykin, B.I.; Kudrina, M.A.; Sysoeva, L.P.; Gazetdinova, N.G.; Neklesova, I.D.; Kitaev, Y.P. Antimicrobial activity of some acyl halide arylhydrazones and carboxylic acid arylhydrazides. *Pharm. Chem. J.* **1980**, *14*, 162–169. [CrossRef]

15. Mohamed, M.F.; Hassaneen, H.M.; Elzayat, E.M.; El-Hallouty, S.M.; El-Manawaty, M.; Saleh, F.M.; Mohamed, Y.; El-Zohiry, D.; Fahmy, G.; Abdelaal, N.; et al. Biological activity, apoptotic induction and cell cycle arrest of new hydrazonoyl halides derivatives. *Anticancer Agents Med. Chem.* **2019**, *19*, 1141–1149. [CrossRef]

16. Rothe, A. Contact dermatitis from N-(α-chlorobenzylidene)phenylhydrazine. *Contact Dermat.* **1988**, *18*, 16–19. [CrossRef]

17. Hegarty, A.F.; Cashman, M.P.; Scott, F.L. The kinetics of nitrilimine formation in base-catalysed hydrolysis of hydrazonyl halides. *J. Chem. Soc. Perkin Trans. 2* **1972**, 44. [CrossRef]

18. Sharp, J.T. Nitrile ylides and nitrile imines. In *Chemistry of Heterocyclic Compounds: A Series of Monographs*; Padwa, A., Pearson, W.H., Eds.; John Wiley & Sons, Inc.: New York, NY, USA, 2003; pp. 473–537. [CrossRef]

19. Caramella, P.; Grünanger, P. *1,3-Dipolar Cycloaddition Chemistry*; Wiley-Interscience: Hoboken, NJ, USA, 1984; Volume 1, pp. 291–392.

20. Frohberg, P.; Drutkowski, G.; Wagner, C. Synthesis and structural assignment of oxanilo-N-arylhydrazonoyl chlorides. *Eur. J. Org. Chem.* **2002**, *2002*, 1654–1663. [CrossRef]

21. Prasad, N.; Sahay, A.; Prasad, J.; Singh, K. Studies on Complex Arylhydrazones. 13. Action of Bromine on 2,3-Dioxo-2-PhenylHydrazono Butyric Acid. *Asian J. Chem.* **1996**, *8*, 357–360.

22. Greb, L.; Lehn, J.-M. Light-driven molecular motors: Imines as four-step or two-step unidirectional rotors. *J. Am. Chem. Soc.* **2014**, *136*, 13114–13117. [CrossRef]

23. Prasad, N.; Sahay, A.; Prasad, J.; Singh, K. Studies on Arylhydrazones. 12. Action of Bromine on Ethylhydrogen Mesoxalate Phenylhydrazones. *Asian J. Chem.* **1996**, *8*, 65–74.

24. Landge, S.M.; Tkatchouk, E.; Benítez, D.; Lanfranchi, D.A.; Elhabiri, M.; Goddard, W.A.; Aprahamian, I. Isomerization mechanism in hydrazone-based rotary switches: Lateral shift, rotation, or tautomerization? *J. Am. Chem. Soc.* **2011**, *133*, 9812–9823. [CrossRef] [PubMed]

25. Beaton, H.G.; Willey, G.R.; Drew, M.G.B. Preparation and hydrogen bonding studies of phenylhydrazone derivatives of alloxan: Crystal and molecular structure of pyrimidine-2(1H),4(3H),5,6-tetraone 5-(2-nitrophenyl)hydrazone. *J. Chem. Soc. Perkin Trans. 2* **1987**, 469. [CrossRef]

26. Zhao, Y.; Truhlar, D.G. Exploring the limit of accuracy of the global hybrid meta density functional for main-group thermochemistry, kinetics, and noncovalent interactions. *J. Chem. Theory Comput.* **2008**, *4*, 1849–1868. [CrossRef] [PubMed]

27. Dunning, T.H. Gaussian Basis Sets for Use in Correlated Molecular Calculations. I. The Atoms Boron through Neon and Hydrogen. *J. Chem. Phys.* **1989**, *90*, 1007–1023. [CrossRef]

28. Woon, D.E.; Dunning, T.H. Gaussian Basis Sets for Use in Correlated Molecular Calculations. III. The Atoms Aluminum through Argon. *J. Chem. Phys.* **1993**, *98*, 1358–1371. [CrossRef]

29. Frisch, M.J.; Trucks, G.W.; Schlegel, H.B.; Scuseria, G.E.; Robb, M.A.; Cheeseman, J.R.; Scalmani, G.; Barone, V.; Petersson, G.A.; Nakatsuji, H.; et al. *Gaussian 16*; Revision A.03; Gaussian, Inc.: Wallingford, CT, USA, 2016.

30. Mardirossian, N.; Head-Gordon, M. ωB97M-V: A combinatorially optimized, range-separated hybrid, meta-gga density functional with vv10 nonlocal correlation. *J. Chem. Phys.* **2016**, *144*, 214110. [CrossRef]

31. Caldeweyher, E.; Bannwarth, C.; Grimme, S. Extension of the D3 dispersion coefficient model. *J. Chem. Phys.* **2017**, *147*, 034112. [CrossRef]

32. Neese, F. Software Update: The ORCA Program System—Version 5.0. *WIREs Comput. Mol. Sci.* **2022**, *12*, e1606. [CrossRef]

33. Peterson, K.A.; Shepler, B.C.; Figgen, D.; Stoll, H. On the spectroscopic and thermochemical properties of ClO, BrO, IO, and their anions. *J. Phys. Chem. A* **2006**, *110*, 13877–13883. [CrossRef]

34. Peterson, K.A. Systematically convergent basis sets with relativistic pseudopotentials. I. Correlation consistent basis sets for the post-*d* group 13–15 elements. *J. Chem. Phys.* **2003**, *119*, 11099–11112. [CrossRef]

35. Peterson, K.A.; Figgen, D.; Goll, E.; Stoll, H.; Dolg, M. Systematically convergent basis sets with relativistic pseudopotentials. II. Small-core pseudopotentials and correlation consistent basis sets for the post-*d* group 16–18 elements. *J. Chem. Phys.* **2003**, *119*, 11113–11123. [CrossRef]

36. Lu, T.; Chen, F. Multiwfn: A multifunctional wavefunction analyzer. *J. Comput. Chem.* **2012**, *33*, 580–592. [CrossRef] [PubMed]

37. García-Revilla, M.; Popelier, P.L.A.; Francisco, E.; Martín Pendás, Á. Nature of chemical interactions from the profiles of electron delocalization indices. *J. Chem. Theory Comput.* **2011**, *7*, 1704–1711. [CrossRef] [PubMed]

38. Outeiral, C.; Vincent, M.A.; Martín Pendás, Á.; Popelier, P.L.A. Revitalizing the concept of bond order through delocalization measures in real space. *Chem. Sci.* **2018**, *9*, 5517–5529. [CrossRef] [PubMed]

39. Hugas, D.; Guillaumes, L.; Duran, M.; Simon, S. Delocalization indices for non-covalent interaction: Hydrogen and DiHydrogen bond. *Comput. Theor. Chem.* **2012**, *998*, 113–119. [CrossRef]
40. Levina, E.O.; Khrenova, M.G.; Tsirelson, V.G. The explicit role of electron exchange in the hydrogen bonded molecular complexes. *J. Comput. Chem.* **2021**, *42*, 870–882. [CrossRef]
41. Gillespie, D.T. A General method for numerically simulating the stochastic time evolution of coupled chemical reactions. *J. Comput. Phys.* **1976**, *22*, 403–434. [CrossRef]
42. Ma, L.; Yuan, Z.; Huang, Z.; Jin, J.; Cao, D.; Guan, R.; Chen, Q.; Sun, X. Reversible regulating of crystal structures based on isomerization of phenylhydrazones. *Chem. Commun.* **2017**, *53*, 12630–12633. [CrossRef]
43. Soave, R.; Colombo, P. Intermolecular C—H...O, Cl...Cl and π–π interactions in the 2-dichloromethyl derivative of vitamin K$_3$. *Acta Crystallogr. C* **2013**, *69*, 1563–1566. [CrossRef]
44. Mantina, M.; Chamberlin, A.C.; Valero, R.; Cramer, C.J.; Truhlar, D.G. Consistent van Der Waals radii for the whole main group. *J. Phys. Chem. A* **2009**, *113*, 5806–5812. [CrossRef]
45. Lommerse, J.P.M.; Price, S.L.; Taylor, R. Hydrogen bonding of carbonyl, ether,and ester oxygen atoms with alkanolhydroxyl groups. *J. Comput. Chem.* **1997**, *18*, 757–774. [CrossRef]
46. Exner, O.; Smolíková, J.; Jehlička, V.; Shawali, A.S. Hydrogen bonding, configuration and conformation of substituted α-oxo oximes and hydrazones. *Collect. Czechoslov. Chem. Commun.* **1979**, *44*, 2494–2506. [CrossRef]
47. Bader, R.F.W. *Atoms in Molecules: A Quantum Theory*; The International Series of Monographs on Chemistry; Clarendon Press: Oxford, UK; Oxford University Press: Oxford, UK, 1994.
48. Novoa, J.J. (Ed.) *Intermolecular Interactions in Crystals: Fundamentals of Crystal Engineering*; Royal Society of Chemistry: London, UK, 2018.
49. Wurmb-Gerlich, D.; Vögtle, F.; Mannschreck, A.; Staab, H.A. Untersuchungen über Schiffsche Basen, VI. Protonenresonanz-Untersuchungen zur syn-anti-Isomerisierung von Iminen. *Justus Liebigs Ann. Chem.* **1967**, *708*, 36–50. [CrossRef]
50. Kerek, F.; Ostrogovich, G.; Simon, Z. Mechanism of the uncatalysed syn–anti-isomerization of imine systems. Part IV. A theoretical study of the influence of substituents. *J. Chem. Soc. B* **1971**, 541–544. [CrossRef]
51. Gálvez, J.; Guirado, A. A Theoretical study of topomerization of imine systems: Inversion, rotation or mixed mechanisms? *J. Comput. Chem.* **2009**, *31*, 520–531. [CrossRef]
52. San-Fabián, E.; Moscardó, F. Cyclobutadiene automerization and rotation of ethylene: Energetics of the barriers by using spin-polarized wave functions. *J. Comput. Chem.* **2014**, *35*, 1356–1363. [CrossRef]
53. Ball, D. Kinetics of consecutive reactions: First reaction, first-order; second reaction, zeroth order. *J. Chem. Educ.* **1998**, *75*, 917. [CrossRef]